UNIVERSIDAD DE INVESTIGACIÓN DE TECNOLOGÍA EXPERIMENTAL YACHAY

Escuela de Ciencias de la Tierra, Energía y Ambiente

TÍTULO: Characterizing infrasound and seismic data from El Reventador volcano to improve hazards monitoring and risk mitigation

Trabajo de integración curricular presentado como requisito para la obtención del título de Geólogo.

Autor:

Perea Armijos Jorge Alexis

Tutor:

Ph.D. Foster Anna Elizabeth

Cotutor:

M. Sc. Ortiz Hugo David

Urcuquí, mayo del 2021

SECRETARÍA GENERAL
(Vicerrectorado Académico/Cancillería)
ESCUELA DE CIENCIAS DE LA TIERRA, ENERGÍA Y AMBIENTE
CARRERA DE GEOLOGÍA
ACTA DE DEFENSA No. UITEY-GEO-2021-00004-AD

A los 25 días del mes de junio de 2021, a las 09:00 horas, de manera virtual mediante videoconferencia, y ante el Tribunal Calificador, integrado por los docentes:

Presidente Tribunal de Defensa	Dra. PIISPA , ELISA JOHANNA , Ph.D.
Miembro No Tutor	Dra. MANDON CELINE LUCIE , Ph.D.
Tutor	Dra. FOSTER ANNA ELIZABETH , Ph.D.

El(la) señor(ita) estudiante **PEREA ARMIJOS, JORGE ALEXIS**, con cédula de identidad No. **1718549866**, de la **ESCUELA DE CIENCIAS DE LA TIERRA, ENERGÍA Y AMBIENTE**, de la Carrera de **GEOLOGÍA**, aprobada por el Consejo de Educación Superior (CES), mediante Resolución **RPC-SE-10-No.031-2016**, realiza a través de videoconferencia, la sustentación de su trabajo de titulación denominado: **Characterizing infrasound and seismic data from El Reventador volcano to improve hazards monitoring and risk mitigation**, previa a la obtención del título de **GEÓLOGO/A**.

El citado trabajo de titulación, fue debidamente aprobado por el(los) docente(s):

Tutor	Dra. FOSTER ANNA ELIZABETH , Ph.D.

Y recibió las observaciones de los otros miembros del Tribunal Calificador, las mismas que han sido incorporadas por el(la) estudiante.

Previamente cumplidos los requisitos legales y reglamentarios, el trabajo de titulación fue sustentado por el(la) estudiante y examinado por los miembros del Tribunal Calificador. Escuchada la sustentación del trabajo de titulación a través de videoconferencia, que integró la exposición de el(la) estudiante sobre el contenido de la misma y las preguntas formuladas por los miembros del Tribunal, se califica la sustentación del trabajo de titulación con las siguientes calificaciones:

Tipo	Docente	Calificación
Miembro Tribunal De Defensa	Dra. MANDON CELINE LUCIE , Ph.D.	8,9
Presidente Tribunal De Defensa	Dra. PIISPA , ELISA JOHANNA , Ph.D.	9,2
Tutor	Dra. FOSTER ANNA ELIZABETH , Ph.D.	8,9

Lo que da un promedio de: **9 (Nueve punto Cero)**, sobre 10 (diez), equivalente a: **APROBADO**

Para constancia de lo actuado, firman los miembros del Tribunal Calificador, el/la estudiante y el/la secretario ad-hoc.

Certifico que *en cumplimiento del Decreto Ejecutivo 1017 de 16 de marzo de 2020, la defensa de trabajo de titulación (o examen de grado modalidad teórico práctica) se realizó vía virtual, por lo que las firmas de los miembros del Tribunal de Defensa de Grado, constan en forma digital*.

PEREA ARMIJOS, JORGE ALEXIS
Estudiante

Firmado electrónicamente por:
JORGE ALEXIS
PEREA ARMIJOS

Dra. PIISPA , ELISA JOHANNA , Ph.D.
Presidente Tribunal de Defensa

Digitally signed by ELISA JOHANNA PIISPA

Dra. FOSTER ANNA ELIZABETH , Ph.D.

ANNA ELIZABETH Digitally signed by ANNA ELIZABETH FOSTER

Dra. MANDON CELINE LUCIE , Ph.D.
Miembro No Tutor

CELINE LUCIE
MANDON
2021.06.25 15:00:07
-05'00'

TERÁN ROSALES, ANDREA YOLANDA

Secretario Ad-hoc

ANDREA
YOLANDA

TERAN ROSALES

Firmado digitalmente por
ANDREA YOLANDA TERAN
ROSALES

-05'00'
Fecha: 2021.06.25 10:16:07

AUTORÍA

Yo, **Jorge Alexis Perea Armijos**, con cédula de identidad 1718549866, declaro que las ideas, juicios, valoraciones, interpretaciones, consultas bibliográficas, definiciones y conceptualizaciones expuestas en el presente trabajo; así cómo, los procedimientos y herramientas utilizadas en la investigación, son de absoluta responsabilidad de el/la autor (a) del trabajo de integración curricular. Así mismo, me acojo a los reglamentos internos de la Universidad de Investigación de Tecnología Experimental Yachay.

Urcuquí, mayo del 2021

Jorge Alexis Perea Armijos

CI: 1718549866

AUTORIZACIÓN DE PUBLICACIÓN

Yo, **Jorge Alexis Perea Armijos**, con cédula de identidad 1718549866, cedo a la Universidad de Tecnología Experimental Yachay, los derechos de publicación de la presente obra, sin que deba haber un reconocimiento económico por este concepto. Declaro además que el texto del presente trabajo de titulación no podrá ser cedido a ninguna empresa editorial para su publicación u otros fines, sin contar previamente con la autorización escrita de la Universidad. Asimismo, autorizo a la Universidad que realice la digitalización y publicación de este trabajo de integración curricular en el repositorio virtual, de conformidad a lo dispuesto en el Art. 144 de la Ley Orgánica de Educación Superior.

Urcuquí, mayo del 2021

Firmado electrónicamente por:
JORGE ALEXIS PEREA ARMIJOS

———————————————

Jorge Alexis Perea Armijos

CI: 1718549866

DEDICATION

I dedicate this work to Mrs. Carmen Beatriz Armijos Armijos, my mother and the pillar of my life. I could not have gotten this far without the unlimited support and unconditional love of the person who has been a mother and father at the same time.

Especially thank to Jesus for his infinite passion and philosophy of love. Thank you for protecting me at every step of my life.

Jorge Perea Armijos

ACKNOWLEDGMENTS

First of all, I want to thank my thesis advisor, Ph.D. Anna Foster for her unconditional scientific and financial support. I couldn't be more grateful to her for all the guidance, consideration, and trust she has put in me. She and the teachers of ECTEA are the best people and teachers I could have ever met.

Many thanks to my co-tutor, Hugo Ortiz, for all the vast knowledge and patience he has shared with me. Thanks for the continuous comments and unconditional help from him. I learned and enjoyed the pleasant experience of the field, from the volcanic deposits of the Tungurahua in Baños to the majesty within the living crater of the Guagua Pichincha. Thanks to the IG-EPN team and the Pontifical Catholic University.

Of course, I want to thank my alma mater, Yachay Tech University. I could not be more indebted to the public institution that welcomed me and elevated me to the universe of science. Infinite thanks to all the Geology knowledge engine, our teachers: Patri, Alysia, Alejandra, Luis Felipe, Jorge, Paul. Special thanks to Jorge Toro for his help and guidance in fieldwork; Celine Mandon for her patience and consideration; Azam Soltani for all the passion and enthusiasm in teaching even in times of pandemic; Elisa Piispa for all the motivation given to the universe of geophysics and geophysics applied both in Ecuador and Colombia, and finally, to Rafael Almeida the best teacher who has motivated and driven me to get my degree, thanks to his selfless support and strict teaching.

I also want to thank the people who briefly passed along this path but left me with great teachings, profe Juan Rosales, profe Javier Arbonaida, profe Eli Rivadeneira, profe Antonio, profe Gallo, profe Camacho, and profe Pablito Medrano. I take great teachings from you.

To my friends, the unforgettable friends of House 26: Bryan Chiguano, Bryan Chamba, Moises Bustamante, Jorge Cardenas, Kevin, Jonathan. My great friends derived from the 26: Jozz, Nadia, Paul, Lu, Ariana, Emilia. To my brother from another mother and eternal companion of the glorious I1-4: Jonathan Vega. Juan Carlos, Gustavo, and Cristian the worst best roommates. To my lifelong friends and siblings: Daniela Caiminagua, Samantha Miranda, Damián, William, Gabo, Boris, Alejo, Dani, Edwin, Wendy, and Bryan. And finally, to my colleagues and geo-friends: Sebastian, Harvey, Andy, María,

Karen, Erika, Danny, Mariela, Mario, Carlos, Joshua, Bladimir, Carlos, Patty, Rubén, Guido and Luis. Each class and field trip was a great adventure!

And last but not least, thanks to the love of my life. Margarita del Rocío, this is also for you; both you and I have been building and growing in various aspects. Thank you for being light and joy in my life. Thank you for your eternal love and your infinite company. The best adventure was being together. I love you.

To my mother and to everyone who believes in me. Endless thanks for making this dream come true.

Honor, Science, and Freedom.

Jorge Perea Armijos

ABSTRACT

Between the provinces of Napo and Sucumbíos 100 km east of Quito lies El Reventador volcano. This volcano is one of the most active volcanoes in the Ecuadorian arc, and represents a major source of hazard, as it is very close to populated areas in the country, as well as to major infrastructure like hydroelectric power plants, roads, and oil pipelines. Currently, volcanologists and geophysicists use infrasound data along with other geophysical measurements like seismicity, deformation, gravity, and thermal cameras to monitor volcanic activity and infer eruption dynamics.

In this project, I study the eruptive mechanisms at El Reventador volcano using infrasound arrays. El Reventador is an excellent target due to its intense and quasi-continuous infrasound activity. I use daily data from May 1 to June 30, 2015, from the infrasound array AZU, which includes three infraBSU microphones and one trillium compact 120 s seismometer connected to a Ref Tek 130 digitizer located 3.8 km from the summit. In addition, I compare the acoustic signals observed with seismic signals.

For the analyses, I used cross-correlation to find periods with coherent signals called detections. In addition, I found the source location of these detections using lag times, then finally grouped detections into events using the back azimuth range belonging to El Reventador. Using different frequency bands to see the source of infrasound, I can identify two primary sources of infrasound: El Reventador volcano and San Rafael waterfall. In general, using second-order Butterworth filter and grouping detections into events can allow characterizing the infrasound signals associated with known eruptive events. The grouped events result in a new local infrasound catalog of El Reventador volcano. The frequency band that best captures El Reventador volcano as an infrasound source is [1-5] Hz. However, higher frequency bands as [10-35] Hz show similarities in the number of events if some parameter values of time such as window length and time are taken into account. With the help of seismic analysis in the same days of acoustic activity records, I demonstrate that emission tremors and explosions precede larger eruptions and lava extrusion phases in El Reventador volcano.

Keywords: infrasound, El Reventador volcano, seismicity, hazards monitoring.

RESUMEN

Entre las provincias de Napo y Sucumbíos, a 100 km al este de Quito se encuentra el volcán El Reventador. Este volcán es uno de los volcanes más activos del arco ecuatoriano, y representa una fuente importante de peligro ya que se encuentra muy cerca de zonas pobladas del país, así como de importantes infraestructuras como centrales hidroeléctricas, carreteras y oleoductos. Actualmente, los vulcanólogos y geofísicos utilizan datos de infrasonidos junto con otras medidas geofísicas como sismicidad, deformación, gravedad y cámaras térmicas para monitorear la actividad volcánica e inferir la dinámica de las erupciones.

En este proyecto, estudio los mecanismos de desgasificación en el volcán El Reventador usando arreglos de infrasonidos. El Reventador es un excelente objetivo por su intensa y casi continua actividad infrasónica. Utilizo datos diarios del 1 de mayo al 30 de junio de 2015 que provienen del arreglo infrasónico AZU, que incluye tres micrófonos infraBSU y un sismómetro trillium compact 120 s conectado a un digitalizador Ref Tek 130 ubicado a 3.8 km de la cumbre. Además, comparo las señales acústicas observadas con las señales sísmicas.

Para los análisis, usé correlación cruzada para encontrar períodos con señales coherentes llamadas detecciones. Además, encontré la ubicación de origen de estas detecciones usando tiempos de retraso para finalmente agrupar las detecciones en eventos usando el rango de backazimut que pertenece a El Reventador. Usando diferentes bandas de frecuencia para ver la fuente del infrasonido, puedo identificar dos fuentes principales de infrasonido: el volcán El Reventador y la cascada San Rafael. En general, el uso del filtro Butteerworth de segundo orden y la agrupación de detecciones en eventos puede permitir caracterizar las señales infrasónicas asociadas con eventos eruptivos conocidos. Los eventos de agrupación dan como resultado un nuevo catálogo de infrasonido local del volcán El Reventador. La banda de frecuencia que encaja perfectamente con el volcán El Reventador como fuente de infrasonidos es [1-5] Hz. Sin embargo, las bandas de frecuencias más altas como [10-35] Hz muestran similitudes en el número de eventos si se tienen en cuenta algunos valores de parámetros de tiempo como la longitud de la ventana y el tiempo. Con la ayuda del análisis sísmico en los mismos días de registros de actividad acústica, los temblores de emisión y las explosiones preceden a erupciones más grandes y a fases de extrusión de lava en el volcán El Reventador.

Palabras clave: infrasonido, volcán El Reventador, sismicidad, monitoreo de peligros.

TABLE OF CONTENTS

TABLE OF FIGURES

TABLES

1. Introduction

1.1 Volcano hazards and monitoring

Active volcanoes are big sources of hazard. In particular, volcanoes that have magmas with intermediate composition and are volatile-rich, such as El Reventador, located in the Sub Andean region of Ecuador, are a considerable source of threat, since magma ascent at these volcanoes can be fast, aseismic, and without much warning (Hall et al., 2004). A well-developed monitoring system is fundamental to reduce risks and should include infrasound monitoring. Infrasound allows us to analyze the behaviour and the eruptive phenomena at El Reventador due to quasi-continuous activity. This eruptive phenomenon can also found in the term: 'degassing' by other authors.

Worldwide, many active volcanoes are constantly monitored. A modern volcano monitoring system consists of optical cameras, ground-based observations of gas flux and geodetic anomalies, remote sensing (Arrowsmith, 2010); thermal monitoring to qualitatively identify lava bodies, and the spatial distribution of temperature (Vallejo, 2018); seismic networks (Alvarado, 2018); and electromagnetic radiation and gas spectroscopy (Johnson, 2011). Unlike volcano seismology, which primarily measures disturbances in the solid earth, infrasound is a direct measure of disturbances in the atmosphere, such as the acceleration of gases.

1.2 Infrasound data

Infrasound is a sound wave with the vibration of frequency lower than the audible spectrum of the human hearing, $< 20\,\mathrm{Hz}$. There are several natural and artificial infrasound sources. Volcanic eruptions, storms, tornadoes, avalanches, and even northern lights are the most common natural sources of this type of wave (Muñoz, 2002). Other sources that perturb the atmosphere are meteors (Garces et al., 2004), waterfalls, thunder, rock falls, lahars, and even volcano echoes (Ortiz et al., 2018), which can be detected by infrasound arrays. Artificial infrasound sources include regular acoustic noise, such as car horns, nuclear explosions (Muñoz, 2002), and reentering spacecraft (Garces et al., 2004). The International Monitoring System (IMS) was constructed in 1996 to monitor and enforce the ban on the testing of nuclear weapons. Hence, a worldwide, global network of seismic, hydroacoustic, infrasound, and radionuclide stations was developed (Fee & Matoza, 2013). This has greatly increased the amount of infrasound data available.

In terms of volcanic sources, many processes produce infrasound. Expanding gas at the atmosphere free surface and accelerations of solid rock can produce infrasound waves (Johnson & Ripepe, 2011), and pyroclastic flows and rockfall release low-intensity infrasonic tremors (Arrowsmith, 2010). Infrasound waves provide valuable information on intense volcano activity due to the proximity to the lower atmosphere. Exploding volcanoes perturb the atmosphere and induce low-frequency sound waves, which can propagate to local, regional, and global distances with low intrinsic attenuation (e.g., Johnson et al., 2006, Ortiz et al., 2020). Infrasound activity of volcanoes is detectable by local infrasound sensors (Johnson & Ripepe, 2011). Infrasound sensors can record all types of perturbations in the atmosphere, such as volcanic gases, long-duration vibrations (tremors) and impulsive bursts (explosions) (Fee & Matoza, 2013). Infrasound waves are recorded when Pyroclastic Density Currents (PDCs) and rockfalls disperse after an eruption (Fee & Matoza, 2013). Pressure oscillations are created from thermodynamic processes when magma rises within the earth. The energy released from these shallow processes may propagate into the atmosphere in the form of acoustic energy.

An infrasound array is a set of acoustic sensors that record acoustic activity. For volcanic monitoring, "local distances" signifies within a radius of 15 km approximately from the volcano (Fee & Matoza, 2013). Infrasound arrays record the acoustic amplitude, measured in pascals. Infrasound arrays recording at local distances record pressures as linear acoustic waves. Within local distances, amplitude fall-off is primarily due to geometric spreading because intrinsic attenuation of acoustic wavelengths is minimal (Johnson & Ripepe, 2011). These signals can be shown as a time series or transformed to frequency spectra, similar to seismic waves.

Some examples of infrasound monitoring worldwide are found in Oshima and Maekawa (2011), who used infrasound and video records to show the infrasonic activity when Merapi-type PDCs and rockfalls were produced in Mount Unzen in Japan. Evers and Haak (2003) used infrasound to trace a meteoric trajectory over the Netherlands on the evening of February 19, 2003. Ripepe et al. (2010), instead, used a single infrasound array to track velocities of PDCs from Soufriere Hills Volcano. Although there are not enough studies of infrasound related to PDCs, it seems that its presence produces significant broadband infrasound associated with turbulent processes, and the investigation of PDCs can help to create better hazard mitigation (Fee & Matoza, 2013). Moreover, 20 000 explosions were identified between 2006 and 2008 on Tungurahua

volcano with an infrasound array located 37 km from Tungurahua. This provides better tracking activity and an improvement in identifying periods of eruptive activity (Johnson, 2011). Infrasound monitoring proved to be really useful in the eruption of March 9, 2005, in Mount St Helens, as this eruption was aseismic and visually obscured by cloud cover (Matoza, 2007), so seismic and visual monitoring methods could not contribute.

Atmosphere dynamics affect the propagation of infrasound in all ranges of observation. As a result, acoustic signals can suffer path distortion. Wind, temperature, and topography are the main factors that affect travel times and propagation path. However, in comparison to seismic signals, which are strongly influenced by topography and variations in the solid earth, infrasound signals are relatively unchanged during propagation (Cannata, 2008). The topography and the distribution of acoustic energy from turbulence are sources of attenuation. Attenuation is the acoustic energy loss in the atmosphere (Fee & Matoza, 2013). This occurs by absorption and geometrical spreading. This absorption can occur during the transfer of energy to heat from kinetic energy or can arise by the excitation of gas molecules. Geometrical spreading, instead, happens by a wavefront expansion. Indeed, geometrical spreading is the primary source of the decrease in the amplitude within local distances (Johnson & Ripepe, 2011; Ortiz et al., 2018). Topography could be a concern near El Reventador, since volcanic landscapes often have pronounced topography, which, as mentioned, can exacerbate attenuation and distortion of sound waves. However, the AZU array is not much affected due to the closeness between the summit of El Reventador volcano and the infrasound sensors.

2. Statement of the problem

El Reventador is one of the most active volcanoes of Ecuador and represents a significant source of hazard. Due to the quasi-continuous infrasound activity of this volcano, it is possible to apply several different monitoring tools to assess the threat of continuous volcanic eruptions. Infrasound sensors are capable of monitoring volcanoes, thunder, meteorites, oceanic waves, and atmospheric conditions. There is a need to understand infrasound events better and build a catalog to understand the activity on the larger eruptions and lava extrusion phases.

3. Objectives

Studying the infrasonic dynamics of El Reventador will allow me to understand the volcanic quiescence and eruptions over long periods of time. Further, this contributes to a better understanding of the behaviour of an active volcano, which could provide new tools for risk mitigation and monitoring hazards.

To address this issue, I will divide this thesis into the following components: Chapters 2 and 3 consist of the background of the project, the summary of the Geology of El Reventador volcano, and its historical eruptions. Chapter 4 consists of the main concepts of infrasound and seismic signals, as well as the relationship between signals and volcanic products. In Chapter 5, I will describe the methods in detail. The main steps of the method are as follows:

- Process data taken from the AZU array located 3.8 km from El Reventador's summit.
- Test several frequency bands and other parameters such as window length, and allow gap to find the ranges that are best associated with different sources of infrasound.
- Based on those tests results, build a catalog of infrasound events, with the source and type of event.

The results of this analysis can be found in Chapter 6, with a comparison of the infrasound event catalog to seismic data and volcanic activity identified by IGEPN and other discussion in Chapter 7.

4. Geological framework

4.1 El Reventador volcano

El Reventador volcano is a volcanic complex located at the foothill of the Eastern Cordillera product of the current subduction between two tectonic plates: the Pacific plate below the South American plate. This andesitic stratovolcano situated in the Amazon region has a horseshoe-shaped caldera and is one of the most active volcanoes in the Ecuadorian arc (Fig. 1). Its exploding activity represents a major source of hazard (Hall et al., 2004). El Reventador volcano is composed of a succession of explosive and effusive products, including pyroclastic material, ignimbrites, lavas and volcanic breccias (Vallejo, 2017), located over the Mesozoic sedimentary Napo Formation. Within the horseshoe-shaped caldera, lava flows have accumulated over the depression left by a debris avalanche. The volcanic products of El Reventador are commonly andesitic. Pyroclastic flows, basaltic-andesitic lava flows (Arnold et al., 2019), and lahars fill the caldera (Lees et al., 2008). The geomorphology of El Reventador volcano has been evolving due to continuous activity through these years.

El Reventador volcano has had at least 16 eruptions since 1541 and most recently reactivated its volcanic activity in 2002, having the strongest eruption on November 3 of the same year with a Volcanic Explosivity Index, VEI 4 (Vélez & Alberto, 2011). This eruption produced an ashfall, which affected the capital of Ecuador, Quito, located 100 km west of the volcano. The closest major community is El Chaco. There are other small communities close to the volcano as El Reventador and Manuel Galindo towns, affected by volcanic ash. Additionally, roads such as E- 45 (Quito – Lago Agrio), farms, and even oil pipelines, such as SOTE y OCP, and the Coca Codo Sinclair hydroelectric power plant, are close enough to be affected by the activity of El Reventador volcano.

The dynamics of eruptions of El Reventador are chiefly the phases of volcanic quiescence and eruptions over long periods of time. These eruptions produce quasi-continuous acoustic activity. Eruptive phases have been characterized mainly by strombolian and vulcanian activity, which result in intense infrasonic activity (Johnson et al, 2006).
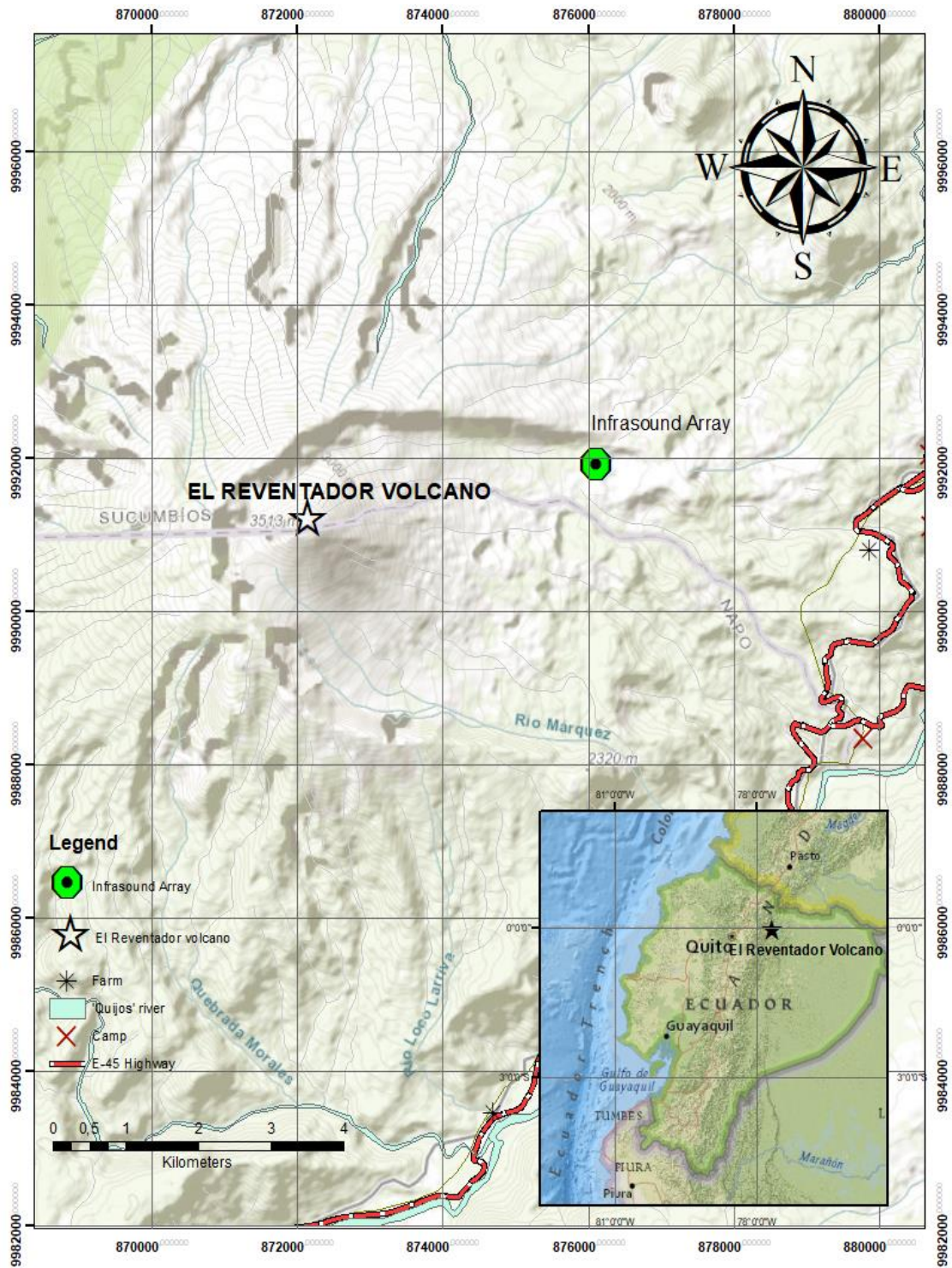
Figure 1. Location of El Reventador volcano and the AZU infrasound array. *Inset***:** Location of El Reventador volcano in the eastern sub-Andean foothills between the provinces of Napo and Sucumbios in Ecuador. *Main*: The AZU infrasound array is located 4 km from the summit of El Reventador, at the foot of the caldera wall.

The most common infrasound signals recorded at El Reventador are low-frequency harmonic signals and emission tremors related to larger eruptions and lava extrusion phases. Currently, The Instituto Geofísico of the Escuela Politécnica Nacional (IG-EPN) is monitoring this volcano continuously through seismic activity, infrared cameras (IGEPN, 2021), satellite radar (Arnold et al., 2019), thermal imaging from REBECA camera and aerial thermal images (Almeida et al., 2019; Vallejo et al., 2019; IGEPN, 2021). This allows us to correlate infrasound information with other direct and remote observations of ash and other eruptive phenomena.

4.2 Previous infrasound work at El Reventador

This work builds on several previous studies of infrasound signals. For instance, Ortiz and Johnson (2013) used two different infrasound arrays between 2006 and 2013 to obtain solid signals from El Reventador and building the first regional infrasound catalog for Tungurahua, Sangay, and El Reventador. Ortiz et al. (2018) used the recording of infrasound waves to study the atmospheric conditions from Volcan Tungurahua's eruptions. Ortiz et al. (2021), using data from 2015 to 2018, also identified El Reventador and San Rafael as the most prominent sources of infrasound. Within local distances, the primary amplitudes of infrasound signals from erupting volcanoes are in the range between 0.4 to 100 Pa. The authors find that signals from El Reventador volcano are typically recorded on the AZU array with a frequency range between 0.7 and 35 Hz. Signals between 1 and 3 Hz are, in general, explosions from El Reventador or San Rafael waterfall signals.

Signals of approximately 15 Hz are identified as rockfalls, and signals of low frequency are variations in the pressure of the atmosphere. The pressure changes with time and altitude. The AZU array records several signals between low and high frequencies, as microbaroms (< 1 Hz) or thunders (~10 Hz). The previous studies show that it is necessary to apply some filters to remove low and high frequencies before attempting to identify volcanic signals. The authors find that using a Butterworth filter between 1 and 5 Hz, with 2-poles, optimizes the frequencies of volcanic signals. Through this band, the signals of El Reventador volcano have a higher correlation than using any other band. This frequency band also removes microbaroms, which are atmospheric infrasonic waves generated on the sea. These sinusoidal waves have frequencies between 0.12 and 0.35 Hz (Ortiz et al., 2018).

5. Data

5.1 Infrasound data

In the atmosphere, acoustic energy propagates as a longitudinal compressional wave. That is, the wave motion through the medium is in the same direction as the propagation of the wave (Fee & Matoza, 2013). The energy propagates at the velocity of sound, *c*. In an ideal gas, the sound speed is $c = \sqrt{\gamma RT}$, where γ is the specific heat ratio, R is the universal gas constant, and T is the temperature (Pierce, 1981). The sound speed in the atmosphere is ~ 340m/s, considering a temperature of 15°C (Cannata et al., 2009; Ripepe, 2002). In the absence of topographic barriers, there is little attenuation of the signal. Attenuation also occurs on infrasound signals during the expansion of the wavefront through the air, producing energy loss due to friction between the air and the sound wave. However, at local distances, it is considered a minor effect (Ripepe, 2002).

5.2 Infrasound data used in this study

In this work, I analyze infrasound and seismic data from May 1, 2015, to June 30, 2015. The data are recorded on the AZU array (Fig. 1). The infrasound array is located 3.8 km from El Reventador's summit, in the range of local distances. In order to consider the waves as plane waves, when working with an array of sensors, the distance between the microphones must be much less than the distance of the array to the source (Ortiz et al., 2018). This is the case for array AZU (15 m << 3.8 km).

In early 2015, the AZU array was installed in the northern flank of the El Reventador (Ortiz et al., 2021). The array consists of three infraBSU microphones and one trillium compact 120 s seismometer connected to 24-bit Ref Tek 130 digitizer. The seismometer was installed 2 meters away from microphone 1. The sensors are continuously recording. I will refer to these sensors as microphone 1 (MC1), microphone 2 (MC2), and microphone 3 (MC3; Fig. 2). An example of an infrasound recording from this array is shown in Fig. 3.
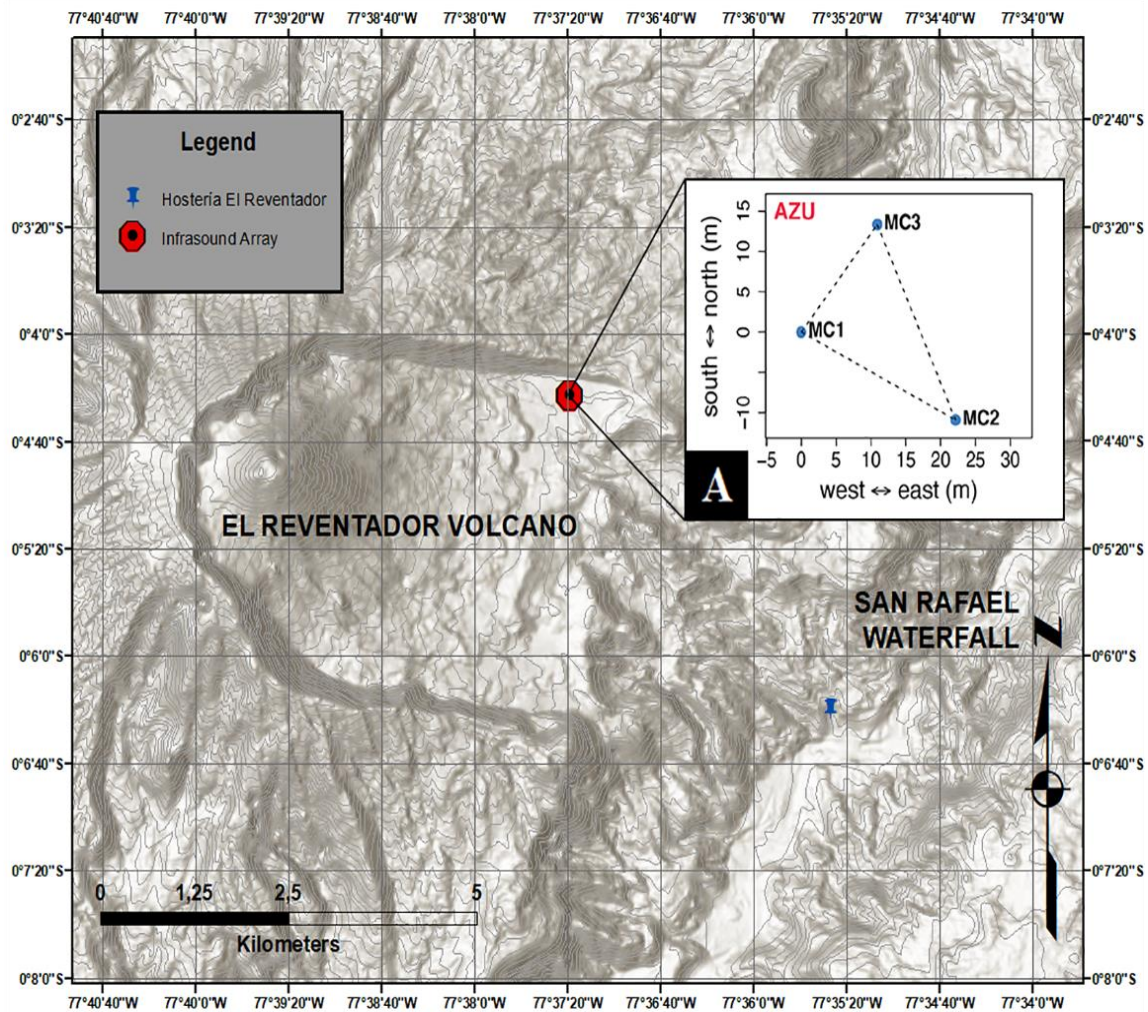
Figure 2. Acoustic–Seismic Monitoring System of El Reventador Volcano and the two largest sources of infrasound events (El Reventador volcano and San Rafael waterfall). The infrasound data for this study comes from station AZU (red circle), and seismic data comes from station AZU and REVN, located in the same place. **(A)** Configuration geometry of the three microphones in the AZU array. The microphones are separated from each other by 15 meters and have an aperture of 25 m. Modified from Ortiz et al. (2021).
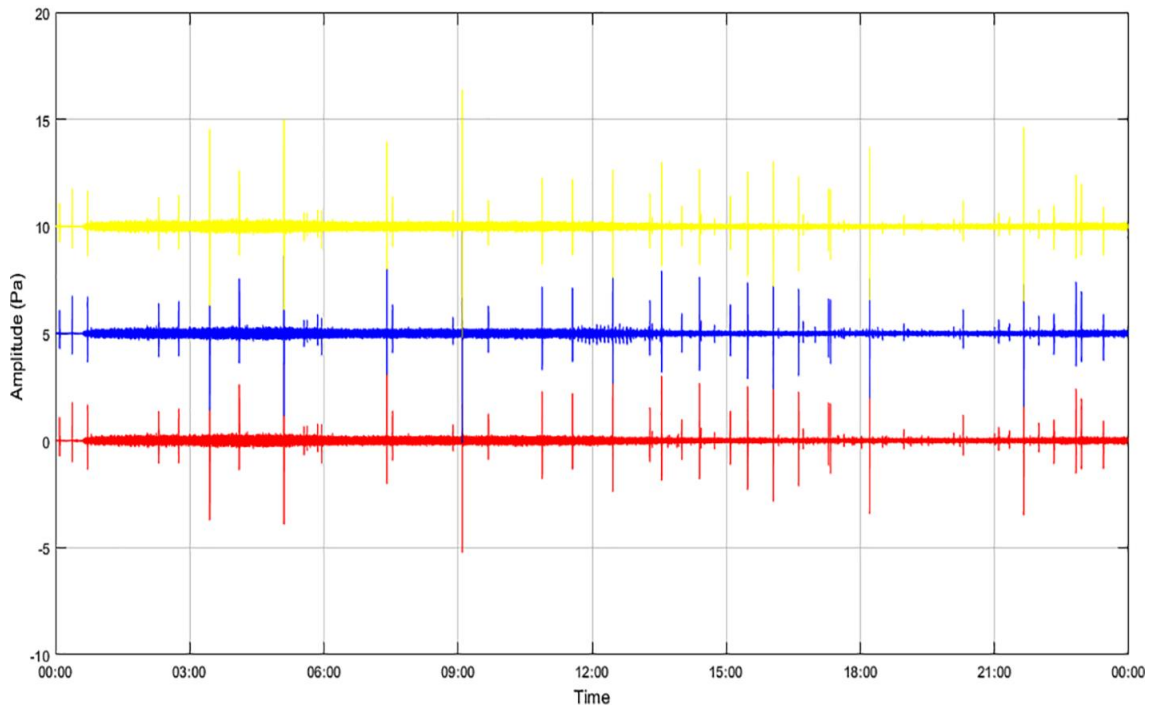
Figure 3. Infrasound signal from El Reventador volcano. This signal is recorded in microphone 1 (yellow), microphone 2 (blue), and microphone 3 (red) of station AZU on May 19, 2015, from 0:00 am to 11:59 pm. This infrasound signal is associated with the movement of a lava flow from the southern flank (IG-EPN, 2015). The station is located 3.8 km from the summit.

5.3 Eruptive activity record

Additional data on the eruptive history of El Reventador volcano come from the daily reports of Instituto Geofísico Escuela Politécnica Nacional (IG-EPN; Instituto Geofísico Escuela Politécnica Nacional, 2020). From these, I compile the number of explosions, emission tremors, long-period events, volcano-tectonic earthquakes and visual thermal images.

According to reports from IG-EPN, between May and June 2015, the main activity of El Reventador volcano was long-period events, explosions, emission tremors, and harmonic tremors (Fig. 4). I sum all the events reported by IG-EPN of these two months. A total of 920 long-period events (LP) were reported in June and 1027 explosions in May (Table 1, Fig.5, Fig.6). Additionally, there was rain reported without the presence of lahars (Annex 1).
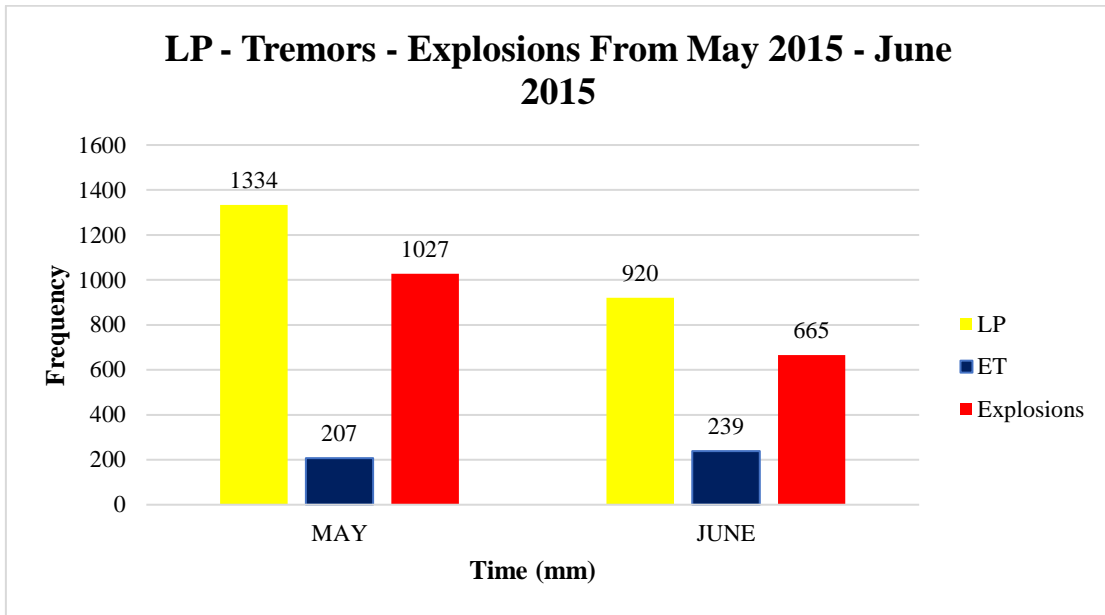
Figure 4. The total number of events reported by IG-EPN between May and June 2015. LP = Long Period Events, ET= Emission Tremors.
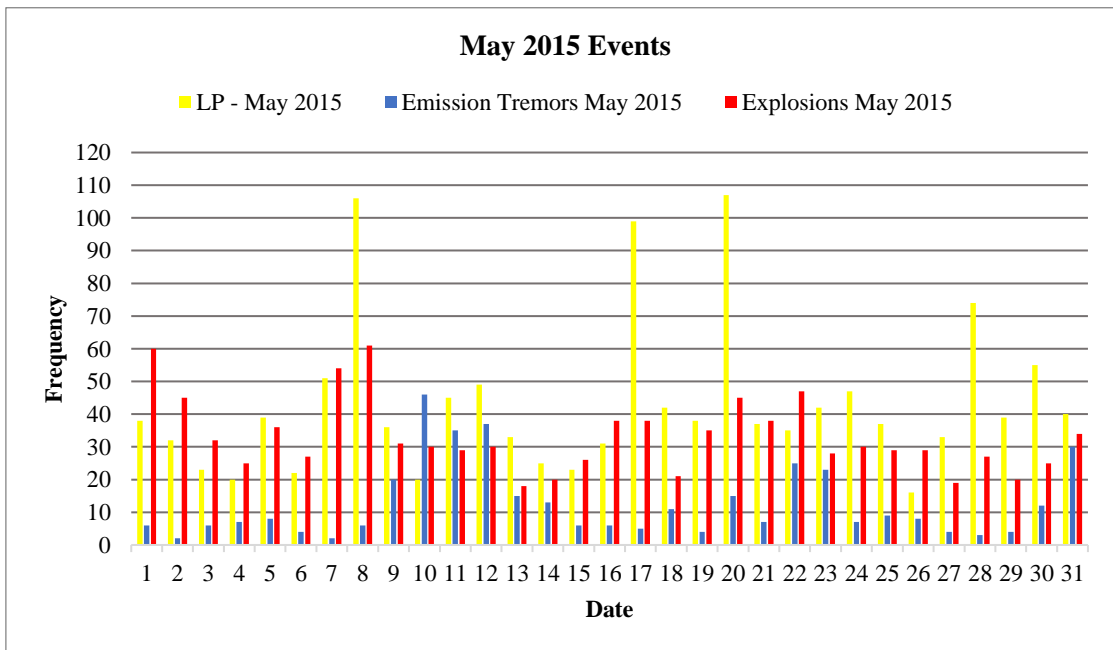
Figure 5. The total number of events reported by IG-EPN in May 2015. LP = Long Period Events.
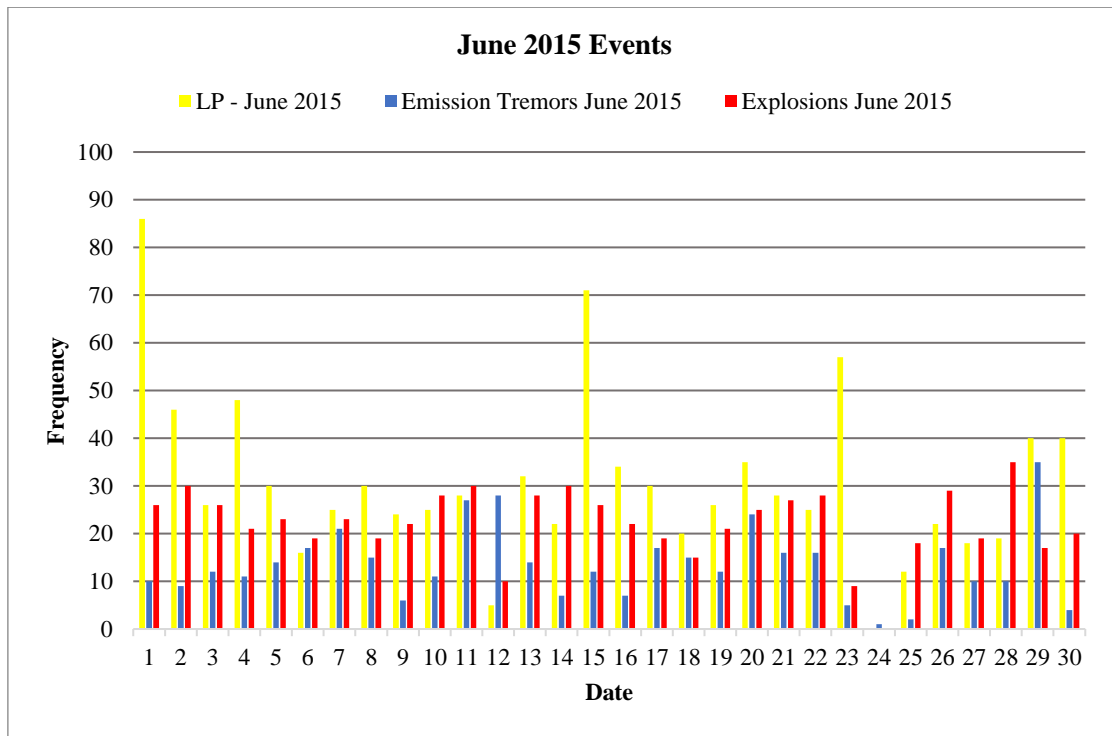
Figure 6. The total number of events reported by IG-EPN in June 2015. LP = Long Period Events.

The number of each event type per day, such as long-period events, explosions, emission, and harmonic tremors, is summarized in Annex 1. Any unusual observations such as the presence of lava, steam, or weather conditions on any particular day, are also noted.

5.4 Seismic data

I use three days of seismic activity (Julian Days 137: May 17, 2015; 138: May 18, 2015; and 139: May 19, 2015) from seismic stations AZU, REVN, and TULM to compare with some of the observed infrasound events. Station AZU has one Trillium Compact 120 s seismometer, and REVN has a broadband seismic sensor. Approximately 90 km from the north of the summit of El Reventador is station TULM (0.72, -77.79), equipped with one Trillium Compact 120 s sensor connected to a Q330S digitizer. This station is part of the *'Red Nacional de Sismógrafos Instituto Geofísico'* (RENSIG) (Alvarado et al., 2018).

Table 1. Events reported by IGEPN

Date	Julian Day	Long Period	Explosions	Tremors	Number of Events
1/5/2015	121	38	60	6	104
2/5/2015	122	32	45	2	79
3/5/2015	123	23	32	6	61
4/5/2015	124	20	25	7	52
5/5/2015	125	39	36	8	83
6/5/2015	126	22	27	4	53
7/5/2015	127	51	54	2	107
8/5/2015	128	106	61	6	173
9/5/2015	129	36	31	20	87
10/5/2015	130	20	30	46	96
11/5/2015	131	45	29	35	109
12/5/2015	132	49	30	37	116
13/5/2015	133	33	18	15	66
14/5/2015	134	25	20	13	58
15/5/2015	135	23	26	6	55
16/5/2015	136	31	38	6	75
17/5/2015	137	99	38	5	142
18/5/2015	138	42	21	11	74
19/5/2015	139	38	35	4	77
20/5/2015	140	107	45	15	167
21/5/2015	141	37	38	7	82
22/5/2015	142	35	47	25	107
23/5/2015	143	42	28	23	93
24/5/2015	144	47	30	7	84
25/5/2015	145	37	29	9	75
26/5/2015	146	16	29	8	53
27/5/2015	147	33	19	4	56
28/5/2015	148	74	27	3	104
29/5/2015	149	39	20	4	63
30/5/2015	150	55	25	12	92
31/5/2015	151	40	34	30	104

Date	Julian Day	Long Period	Explosions	Tremors	Number of Events
1/6/2015	152	86	26	10	122
2/6/2015	153	46	30	9	85
3/6/2015	154	26	26	12	64
4/6/2015	155	48	21	11	80
5/6/2015	156	30	23	14	67
6/6/2015	157	16	19	17	52
7/6/2015	158	25	23	21	69
8/6/2015	159	30	19	15	64
9/6/2015	160	24	22	6	52
10/6/2015	161	25	28	11	64
11/6/2015	162	28	30	27	85
12/6/2015	163	5	10	28	43
13/6/2015	164	32	28	14	74
14/6/2015	165	22	30	7	59
15/6/2015	166	71	26	12	109
16/6/2015	167	34	22	7	63
17/6/2015	168	30	19	17	66
18/6/2015	169	20	15	15	50
19/6/2015	170	26	21	12	59
20/6/2015	171	35	25	24	84
21/6/2015	172	28	27	16	71
22/6/2015	173	25	28	16	69
23/6/2015	174	57	9	5	71
24/6/2015	175			1	1
25/6/2015	176	12	18	2	32
26/6/2015	177	22	29	17	68
27/6/2015	178	18	19	10	47
28/6/2015	179	19	35	10	64
29/6/2015	180	40	17	35	92
30/6/2015	181	40	20	4	64

Each day has the total number of events including long-period events, explosions, and tremors.

6. Methodology

In this section, I identify events and their locations related to the infrasound of the El Reventador volcano. In total, four steps are used in this study and have been tested with infrasound data of two months. I filter daily acoustic data, and cross-correlate the signals from the three microphones to find periods with high similarity, termed detections. To find the source location of these detections, I use the minimal differences in the arrival times between the microphones of the array from the cross-correlation. Once I have these arrival time differences, I can find the source direction using the Inversion method or Grid Search method. Finally, I group the detections into events considering a specific range of back azimuth associated with El Reventador volcano.

A new change to the methodology in this study is the zero-phase filtering, which effectively sees if there is some phase distortion and is used as a filter after the processing step. Otherwise, I follow the methodology of Ortiz et al. (2018).

6.1 Cross –Correlation and detections of coherent energy

Considering a planar wavefront, I calculate wave travel times (lag times) between microphones using cross-correlation. First, I filter signals between [1-5] Hz using a second-order Butterworth filter in a Matlab code; this is done to differentiate volcanic signals from other sources such as rockfalls, waterfalls, thunder, or microbaroms based on their frequency content. Then, I divide the one-day long signals into 5-second consecutive windows with an overlap of 33% before performing cross-correlation (Fig. 7). Cross-correlation permits us to obtain travel time differences among different microphones, which can be related to sound speed using the slowness vector, $\vec{S}$. The modulus of $\vec{S}$ is equal to:

$$|\vec{S}| = \frac{1}{c}$$

Where, c is the speed of sound. The cross-correlation also provides a quantitative measure of the similarity of the signals. I can then use the similarity in the frequencies, velocity, and lag time to determine if the time window contains a coherent infrasound signal, termed a detection (Ortiz et al., 2018).
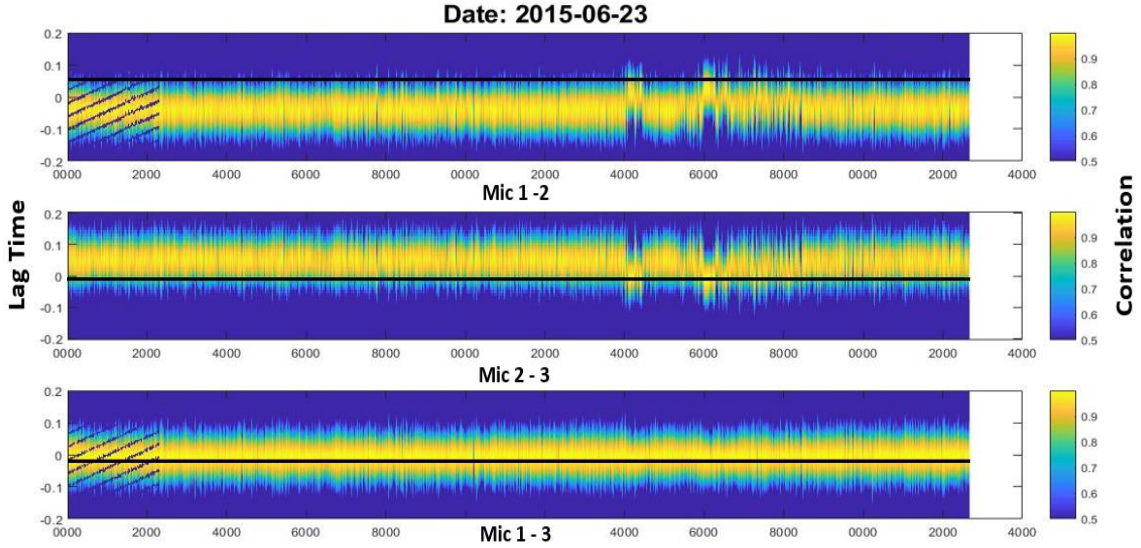
Figure 7. Lag times between microphones for June 23, 2015. The higher the correlation, the more intense the color is (yellow). The black straight line indicates the theoretical wave travel time between microphones. The lag time is the difference of arrival between two microphones (Mic 1-2: Microphone 1 and 2. Mic 2-3: Microphone 2 and 3. Mic 1-3: Microphone 1 and 3). If the lag time is negative, the signal is delayed; if the lag time is positive, the signal is advanced.

To assess high waveform similarity between channels and the quality of lag times, I use a correlation coefficient threshold value, and the consistency criterion (Cansi, 1995). The consistency criterion sets a threshold for reliability. The consistency criterion between two sensors assesses whether there are lag times from cross-correlation functions without a unique well-defined maximum (e.g., Ortiz et al., 2018; Cansi, 1995). For three sensors, the consistency criterion is:

$$\Delta t_{21} + \Delta t_{31} - \Delta t_{23} = 0$$

Where Δt_{21} is the difference between wave travel time to the sensors 1 and 2 from the source, Δt_{31} is the difference between wave travel time to the sensors 3 and 1 from the source, and Δt_{23} is the difference between wave travel time to the sensors 2 and 3 from the source.

6.2 Backazimuth determination: Inversion and Grid Search methods

After finding a detection in a given time window, I need to locate the source of that signal. Since the waves travel with a relatively constant velocity through time, I can use the simple expression:

$$t = \frac{d}{v}$$

Where time (t), is equal to distance (d) over velocity. Knowing that: $t_1 = \vec{s} \cdot \vec{r_1}$, where $\vec{r_1}$ is the unit vector from the source to the sensor 1 and $\vec{s}$ the slowness vector. The projection of S along $\vec{r_1}$ is what I am looking for. Assuming the simplest case that both are collinear I would obtain: $t_1 = |\vec{s}| \cdot |\vec{r_1}| \cos \theta$, where θ is the back azimuth angle.

$$t_2 - t_1 = \vec{s} \cdot \vec{r_2} - \vec{s} \cdot \vec{r_1}$$

$$\Delta t_{21} = \vec{S} \cdot (\vec{r_2} - \vec{r_1})$$

With this model I can find which direction the signal is coming from. With three stations (microphones) I can measure the relative travel time with the following:

$$\Delta t_{21} = \vec{S} \cdot (\vec{r_2} - \vec{r_1})$$

$$\Delta t_{31} = \vec{S} \cdot (\vec{r_3} - \vec{r_1})$$

$$\Delta t_{23} = \vec{S} \cdot (\vec{r_2} - \vec{r_3})$$

Finally, the vector slowness of $\vec{S}$ needs to be calculated. The vector $\vec{S}$ is defined as:

$$\vec{s} = \vec{s_{x\hat{\imath}}} + \vec{s_{y\hat{\jmath}}}$$

And applying the dot product results in (this is known as dependency):

$$\begin{pmatrix} \Delta t_{21} \\ \Delta t_{31} \\ \Delta t_{23} \end{pmatrix} = \begin{pmatrix} x_2 - x_1 & y_2 - y_1 \\ x_3 - x_1 & y_3 - y_1 \\ x_2 - x_3 & y_2 - y_3 \end{pmatrix} \begin{pmatrix} s_x \\ s_y \end{pmatrix}$$

$$d = G * m$$

Where G is a Jacobian matrix, m is the parameters vector, and d is the parameters vector. Therefore, I must get the inverse of the matrix, but since the matrix is not square, I need to multiply the matrix by its transpose.

$$G^T d = G^T \cdot G \cdot m$$

$$(G^T \cdot G)^{-1} G^T d = I \cdot m$$

This process is known as an inverse problem (Ortiz et. al, 2018). However, another approach is to treat it as a forward problem, using a grid search method, testing multiple combinations. Grid search uses several different synthetic distributions and probes which one is the best match with the observations to find the most likely infrasound source location.

$$\vec{\Delta r} = \vec{r_2} - \vec{r_1}$$

Knowing that, $\vec{r_2}$ is the unit vector from the source to the sensor 2, $\vec{r_1}$ is the unit vector from the source to the sensor 1. The projection of S along $\vec{r_1}$ is what I seek. I tested both methods, but in this study, I used a grid search procedure with the requirement that one point in the 3-D space has to be the source.
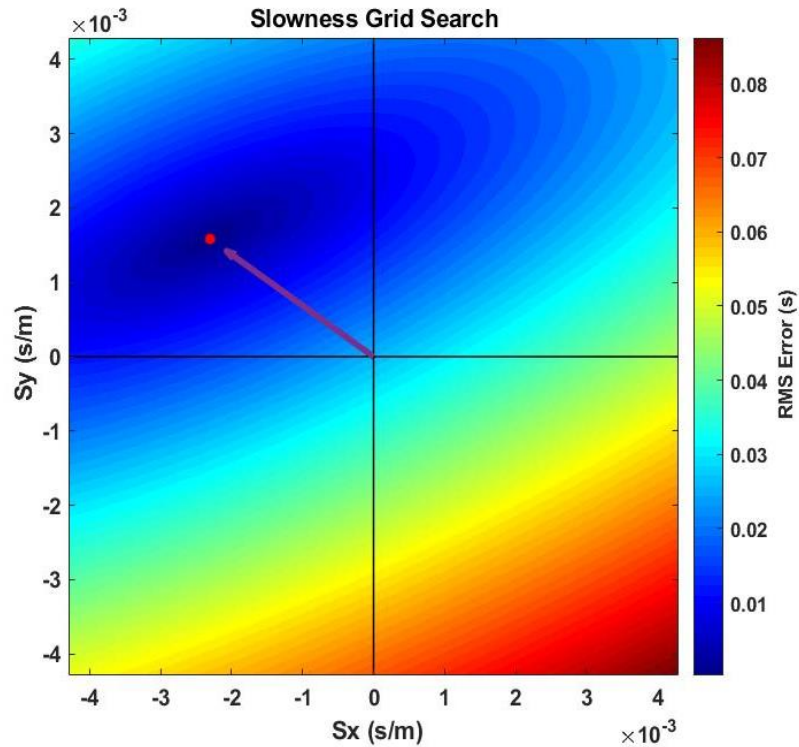

Figure 8. Example of the slowness grid search of an infrasound signal taken on May 18, 2015; from 00:01:00 am to 23:59:00 pm. The warmer color indicates a greater error. The signal taken from 2 microphones shows the direction and slowness.

6.3 From Detections to Events

Afterward, if there are detections, I need to select only the detections from El Reventador volcano, and consolidate them into events. I set a range of allowable backazimuth directions between 250° and 270°, which corresponds to El Reventador (Fig. 9). Then, I define a gap value in seconds. This gap will be the allowed time between detections within an ongoing event. Once I find a detection in the selected back azimuth range, I define a new event with a start time. The event continues as long as there are detections; after a period of time with no detections longer than the permitted gap, the end time of the event is defined. This process is repeated for all of the infrasound data. Finally, I get a matrix with the events with the start time, duration, end time, and the back azimuth. Fig. 10 shows an example of detections grouped into a single event at El Reventador volcano.
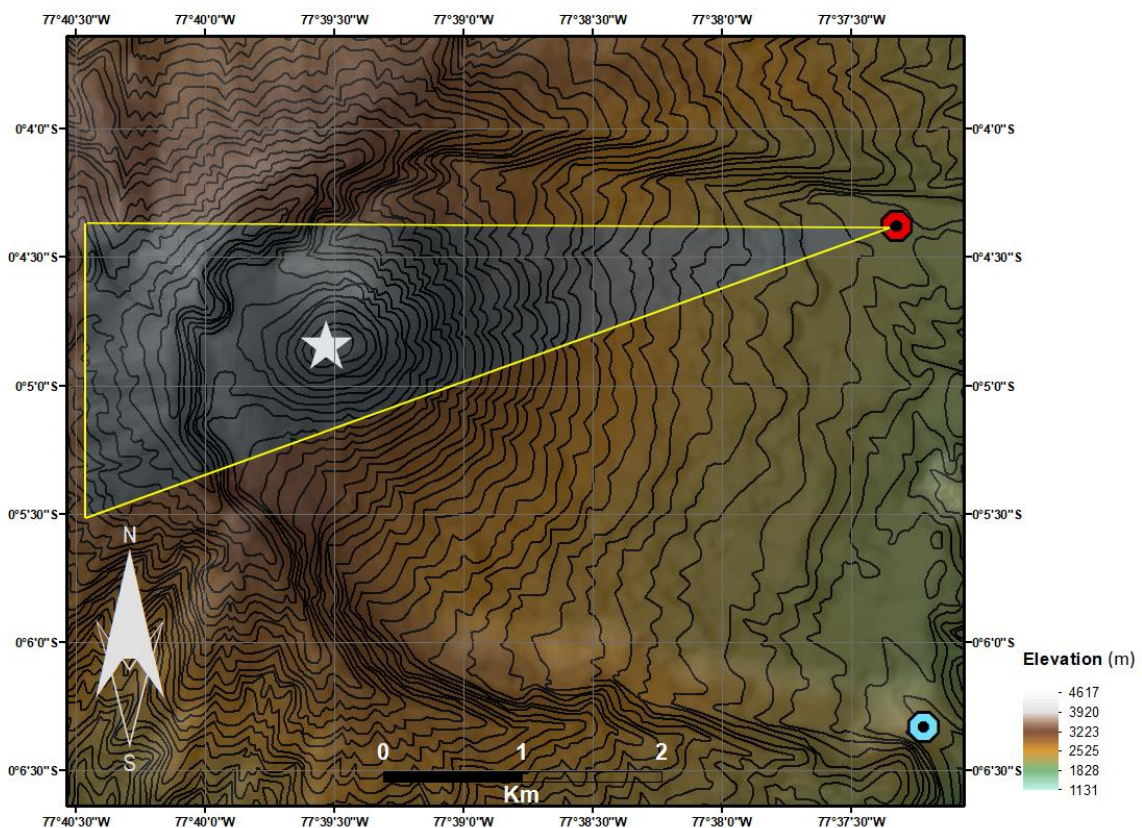
Figure 9. Hillshaded digital elevation model (DEM) showing the back azimuth range of El Reventador volcano. The white star is the summit of the volcano located at approximately 3500 m.a.s.l. The shaded triangle is the back azimuth range (250° to 270°). The red dot is the infrasound array (AZU station), and the light blue is the seismic station (REVS station).
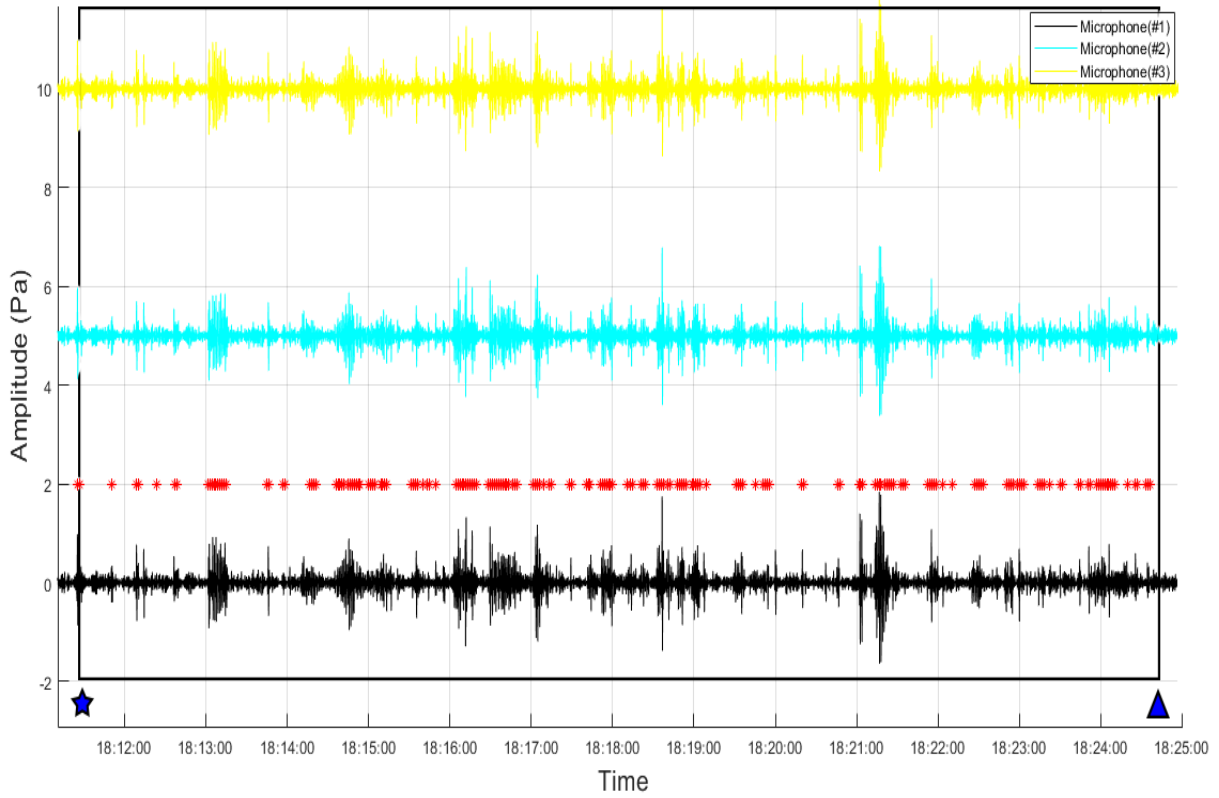
Figure 10. Detections (red asterisks) grouped into an infrasound event (black box) of El Reventador volcano on June 23, 2015. The blue star is the start time and the blue triangle is the end time. The signals were recorded between 18:11:30 and 18:24:40 [hh:mm:ss].

7. **Results**

7.1 Parameter selection

Parameters that can be adjusted in this methodology are the frequency band, correlation threshold, consistency criterion, time window length, and the allowed time gap between detections. The goal in adjusting these parameters is to find the combination that results in the largest number of detections associated with the source of interest (El Reventador), while converging on a stable number of events. I first applied various frequency bands to see the effect on the number of detections from each source of infrasound. In general, I observe two principal sources of infrasound: El Reventador volcano and the San Rafael waterfall.

In Fig. 11, four histograms of the same day are shown. Several frequency bands were used to see the signals of sources around the array. If the frequency band is between [0.7-3] Hz, it is possible to see the signal associated with San Rafael waterfall; getting approximately 1350 detections during that day; this is the maximum number of detections, which also are coherent infrasound signals. If the frequency band is between [10-35] Hz, detections located in the direction of El Reventador volcano are shown. Further, both signals from the San Rafael waterfall and El Reventador volcano can be displayed at the same time if the frequency band is between [4-16] Hz.
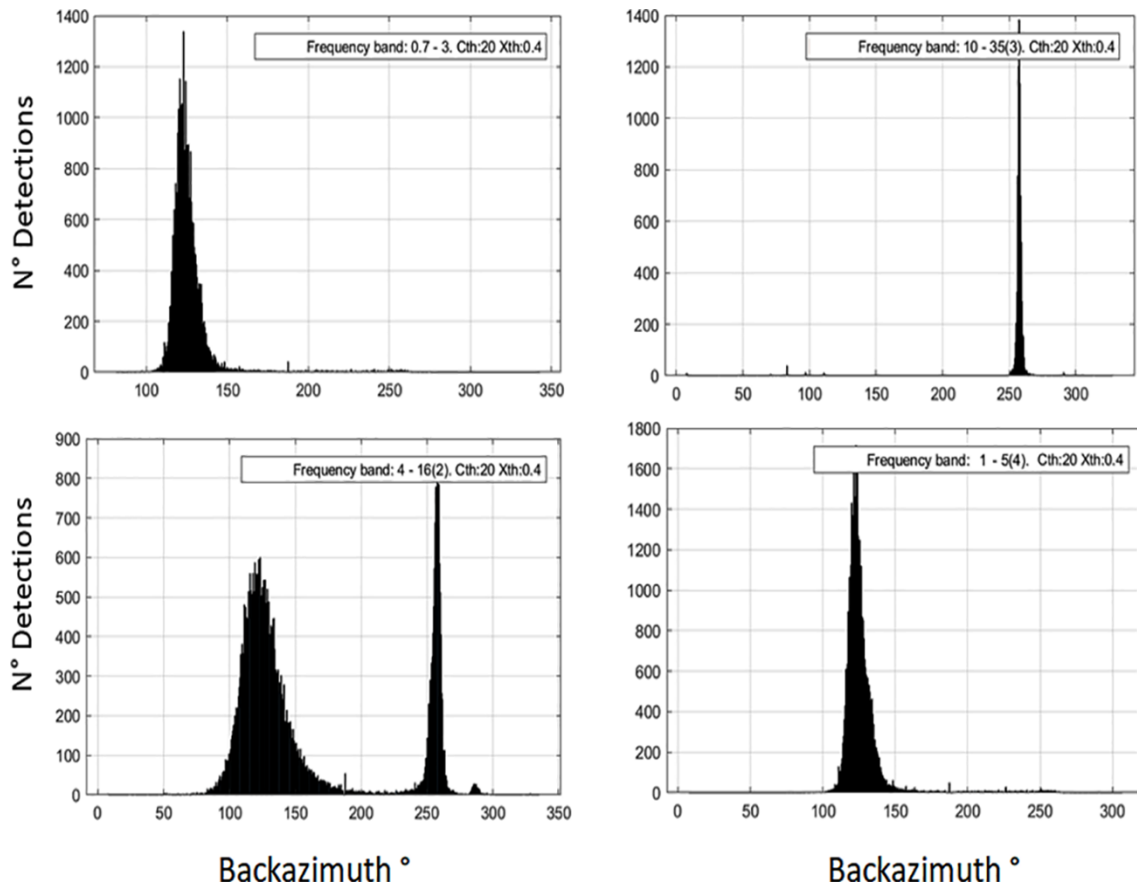
Figure 11. Histograms of back azimuth from sources of infrasound around the AZU array for different frequency bands. The typical back azimuth of El Reventador volcano is 260°, and San Rafael waterfall 120-130°.

I can also modify the consistency criterion ('cth') and the threshold value ('xth'). If I reduce each of these by half (cth = 10 and xth = 0.2), I find approximately the same number of detections from the back azimuth of San Rafael waterfall, and approximately 40% more detections from the back azimuth of El Reventador, however, the reliability of these detections is lower.

Additionally, I need to select a window length, which is the range of time in seconds to test for detections. In general, I observe that if I set a window length of 3 seconds or 6 seconds, the final events found are similar. If I use a 6 seconds window length, the number of events decreases, although not considerably. Finally, I must select the amount of time in seconds allowed between detections within an ongoing event, or a gap. If I increase the size of the gap, I get a smaller number of events (as more detections are grouped into the same event). Table 2 shows the differences in the number of events using two frequency ranges and changing the parameters of window length and gap. Nine

hundred thirty-six events were found on Julian day 174 using the [10-35] Hz frequency range. By contrast, I get 633 fewer events, 936-633 = 303, if I use the range between [1-5] Hz, both frequency ranges using the same window length and gap. However, on most days, there is not a big difference in the number of events for the two different frequency bands [10-35] Hz and [1-5] Hz. On Julian day 180, 56 events were detected using the first frequency range ([10-35] Hz), and 55 events using the second frequency range ([1-5] Hz), with only one event of difference.

Fig. 12A and Fig. 12B show the same infrasound signal but considering a different value of gap. The results show three events (which belongs to 259°, 258°, and 260° back azimuth) in one minute if I use a value of a gap of 10 seconds; instead, if I use a value of a gap of 60 seconds, I can see only one event (which belongs to 259° back azimuth) in one minute. However, if I decrease the gap in some signals, I can get some events not very clear, which in turn will be the same event if I increase enough value of the gap. For example, on Julian day 146 (May 26, 2015), I count four events with back azimuth of 258°, 260°, 256°, and 262° respectively if I use a gap of 20 seconds (Fig. 13B), but If I use a gap of 10 seconds, I will see two extra events that are not very clear (Fig. 13A). Certainly, I need to set a large enough value of the gap manually to avoid splitting events.
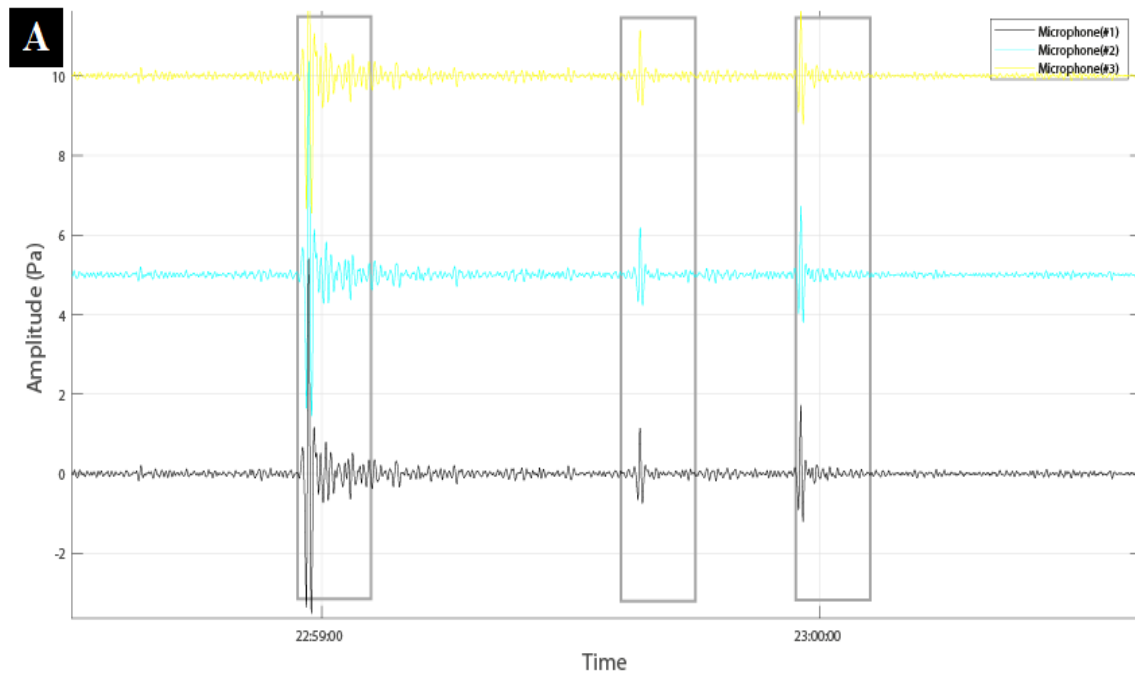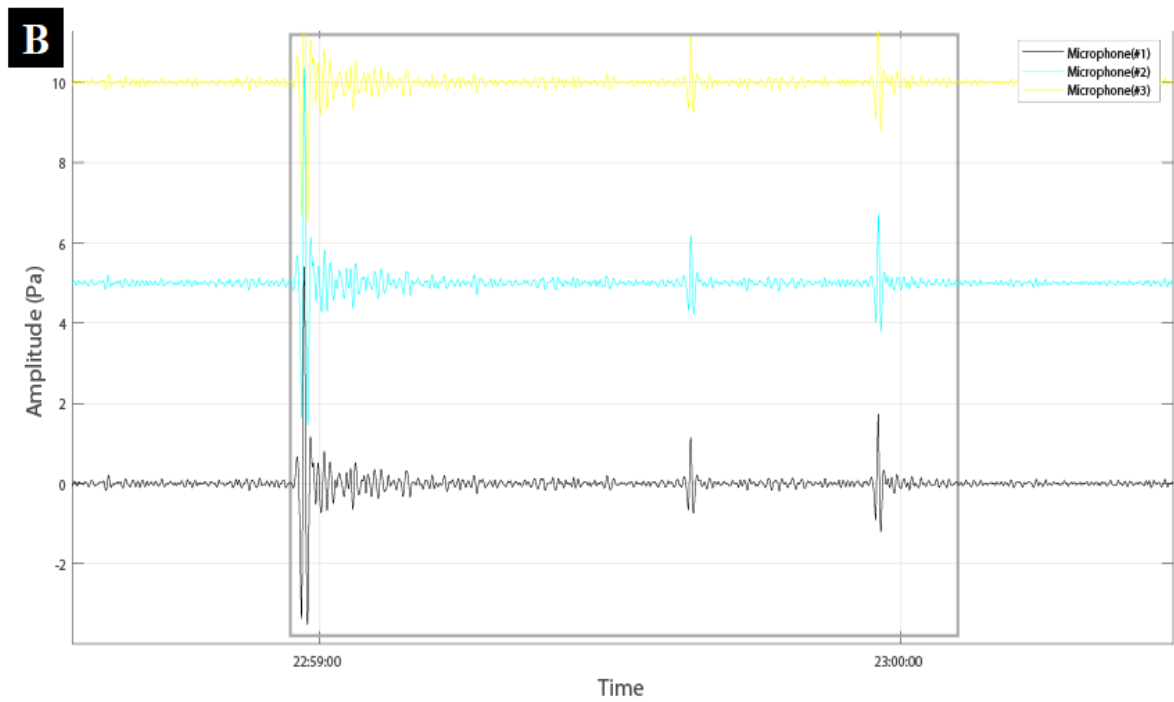
Figure 12. Infrasound signals from El Reventador volcano on Julian day 145 (May 25, 2015), with 259° back azimuth. (A) Three events in one minute in the interval between 22h59 to 23h00, grouped using a gap of 10 s. (B) One event in one minute in the interval of 22h59 to 23h00, grouped using a gap of 60 s.

25
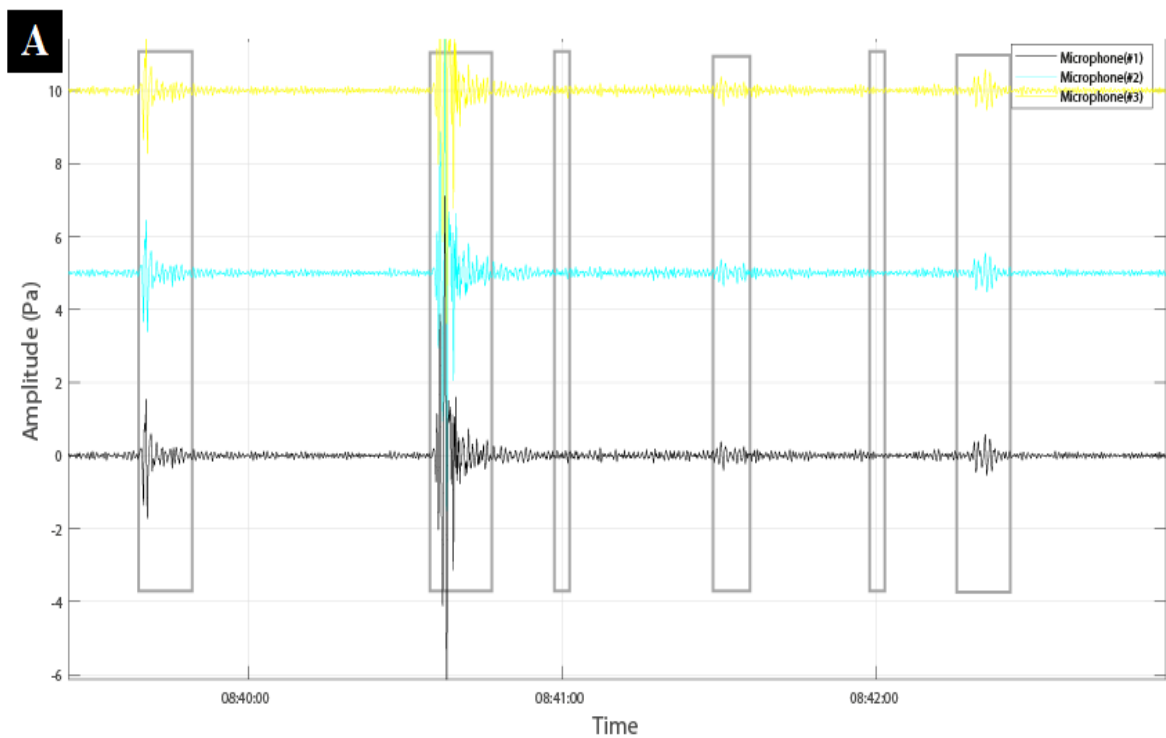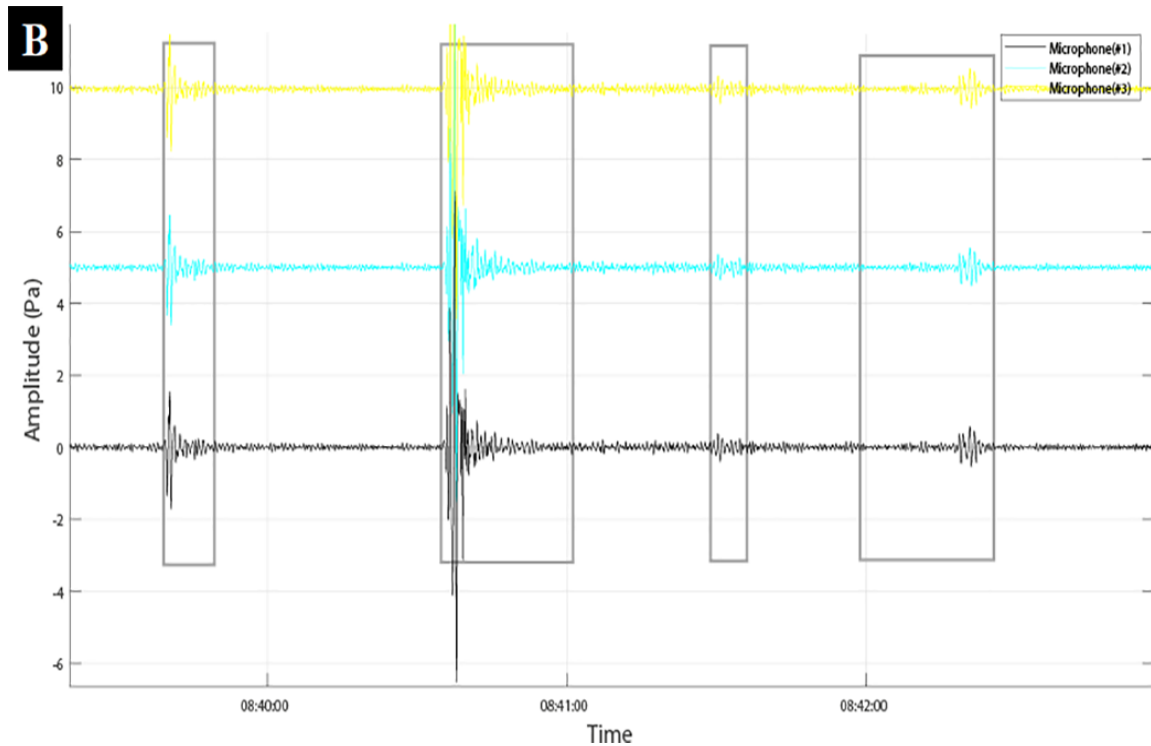
Figure 13. Infrasound signals from El Reventador volcano on day Julian day 146 (May 26, 2015) with 258° back azimuth. **(A)** Six events in three minutes in the interval of 08h39 to 08h42, grouped using a gap of 10 s. **(B)** Four events in three minutes in the interval between 08h39 am to 08h42 am, grouped using a gap of 20 s.

I calculated a different number of events if I changed the frequency range, the window length, and the allowed gap (Fig. 14), (Fig. 15). To illustrate this, first, I got the unfiltered infrasound data from Julian day 174 in 55 minutes from 17:35 to 18h30. After applying the parameters, I got 44 events in this period in the frequency range of [10-35] Hz; instead, I got only 16 events in the same period, but using the frequency range [1-5] Hz.

26
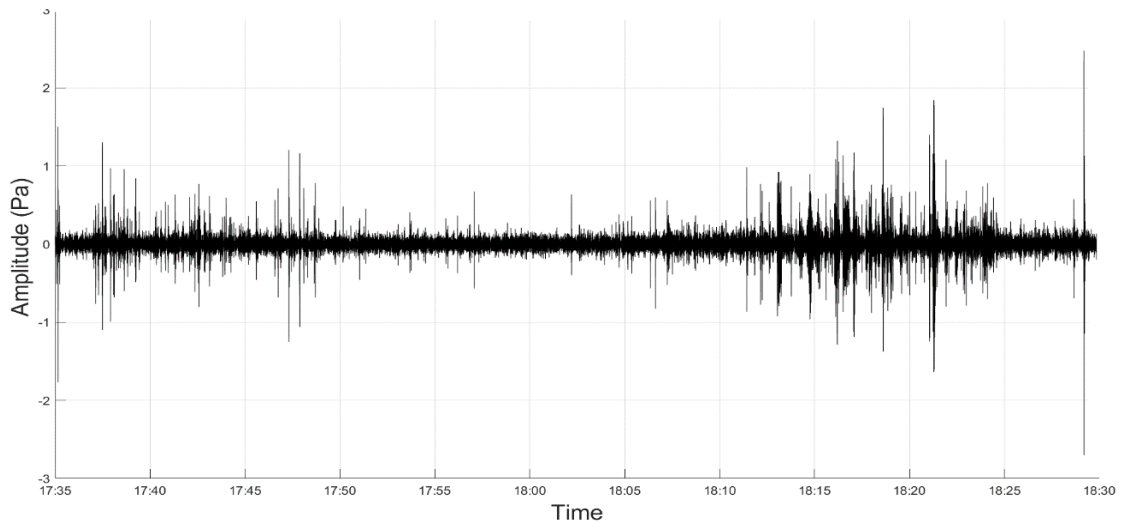
Figure 14. Unfiltered infrasound data of the Julian day 174 (June 23, 2015). The image shows the Microphone 1 getting infrasound data between 17:35 to 18:30.
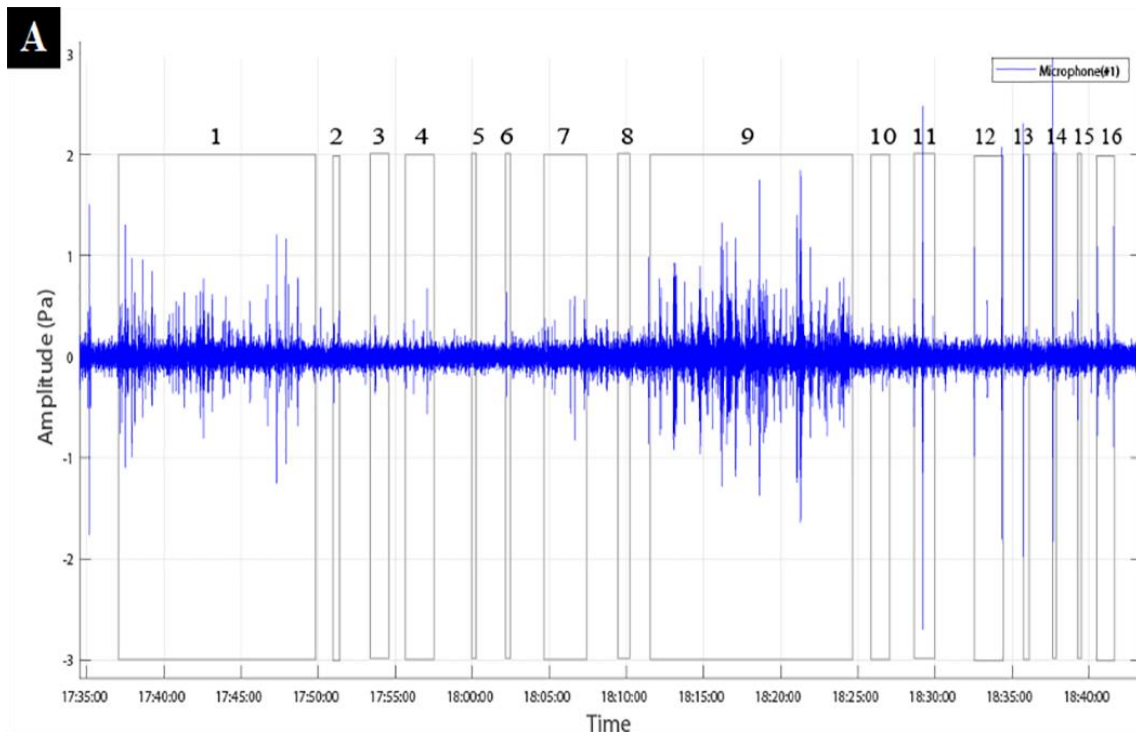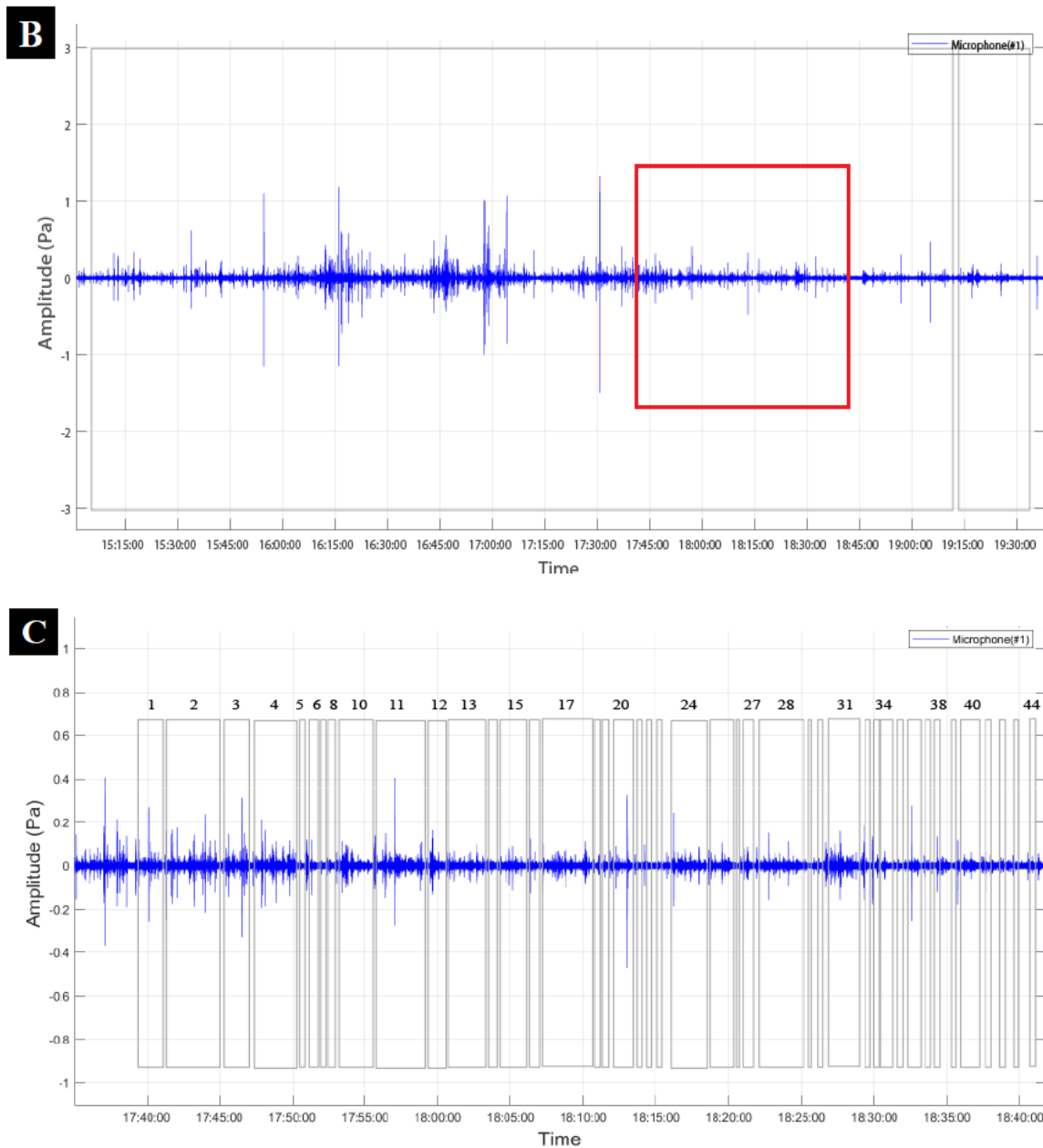
Figure 15. The number of events found on Julian day 174 (June 23, 2015) using different parameters settings. (A) 16 events were counted applying the frequency range [1-5] Hz using a window length of 3 seconds and an allowed gap of 60 seconds in the time between 17:35 to 18:30. (B) The red box shows the same range of time, between 17:35 to 18:30; in that box one ongoing event is counted, which is part of the event between 15:10 to 19:10. The parameters applied in this case were a frequency range between [10-35] Hz, using a window length of 3 seconds and an allowed gap of 60 seconds. (C) 44 events were counted with the frequency range between [10-35] Hz, using a window length of 3 seconds and an allowed gap of 10 seconds. I can see the decrease of amplitude applying this frequency band.

I seek to quantify a consistent number of events considering the number of coherent infrasound signal detections. Hence, I choose the final parameters as values that allow detecting the high number of events from the expected sources. The frequency band that resulted in the most significant number of detections from El Reventador volcano is [10-35] Hz. The [1-5] Hz frequency band filter better captures the San Rafael waterfall. However, I build the infrasound catalog based on previous work related to infrasound detections of Ecuadorian volcanoes, using the [1-5] Hz band. This is because the best conditions to detect events are on low frequencies due the most energy is content on [0.5-5] Hz. Low frequencies can guarantee better the characterization of the signal from El Reventador volcano.

Table 2. Numbers of events of El Reventador volcano for different parameter settings

Date	Julian Day	Events									
		[10-35] (3){10}	[1-5] (3){10}	[1-5] (3){20}	*[1-5] (3){60}*	[1-5] (3){90}	[10-35] (6){10}	[1-5] (6){10}	[1-5] (6){20}	[1-5] (6){60}	[1-5] (6){90}
23/6/2015	174	936	303	217	*115*	91	659	187	146	89	74
24/6/2015	175	700	120	113	*95*	85	520	71	70	66	60
25/6/2015	176	87	33	32	*32*	32	79	21	20	20	20
26/6/2015	177	68	34	34	*34*	34	50	27	27	25	24
27/6/2015	178	84	64	60	*58*	57	72	58	56	54	53
28/6/2015	179	119	46	46	*40*	37	72	43	43	39	37
29/6/2015	180	56	55	50	*40*	39	49	46	42	39	38
30/6/2015	181	57	44	40	*40*	40	41	40	39	39	39

Number of events using different frequency ranges and parameters of time. The parameters given are [frequency range in Hz], (window length in seconds) {allowed gap between detections for a given event, in seconds}.

7.2 Infrasound catalog

The infrasound catalog (Table 3) was built using the frequency range of [1 5] Hz, a window length of (3) seconds, an allowed gap {60} seconds, a consistency criterion of cth = 20, and the threshold value xth = 0.4. A total of 2677 events were recorded in May 2015, with Julian Day 137 (May 17, 2015) being the day with the most events recorded. On this day, I counted 150 events. I counted 1789 events in June 2015. The day with the

most events recorded in June was Julian Day 174 (June 23, 2015), with 115 events in total. In general, I get between 32 to 150 events per day during two months of activity.

Table 3. Infrasound catalog of the events of El Reventador volcano using the frequency range [1-5] Hz, a window length of 3 s and a gap value of 60 s.

Date	Julian Day	Number of events	Date	Julian Day	Number of events
1/5/2015	121	111	1/6/2015	152	70
2/5/2015	122	126	2/6/2015	153	92
3/5/2015	123	125	3/6/2015	154	76
4/5/2015	124	73	4/6/2015	155	72
5/5/2015	125	108	5/6/2015	156	93
6/5/2015	126	62	6/6/2015	157	62
7/5/2015	127	98	7/6/2015	158	38
8/5/2015	128	147	8/6/2015	159	63
9/5/2015	129	125	9/6/2015	160	86
10/5/2015	130	92	10/6/2015	161	62
11/5/2015	131	47	11/6/2015	162	76
12/5/2015	132	65	12/6/2015	163	54
13/5/2015	133	46	13/6/2015	164	54
14/5/2015	134	59	14/6/2015	165	58
15/5/2015	135	80	15/6/2015	166	51
16/5/2015	136	104	16/6/2015	167	49
17/5/2015	137	150	17/6/2015	168	45
18/5/2015	138	112	18/6/2015	169	20
19/5/2015	139	76	19/6/2015	170	55
20/5/2015	140	103	20/6/2015	171	52
21/5/2015	141	111	21/6/2015	172	59
22/5/2015	142	66	22/6/2015	173	48
23/5/2015	143	50	23/6/2015	174	115
24/5/2015	144	45	24/6/2015	175	95
25/5/2015	145	41	25/6/2015	176	32
26/5/2015	146	58	26/6/2015	177	34
27/5/2015	147	74	27/6/2015	178	58
28/5/2015	148	76	28/6/2015	179	40
29/5/2015	149	85	29/6/2015	180	40
30/5/2015	150	71	30/6/2015	181	40

31/5/2015	151	91	

7.3 Seismic data

I have continuous seismic data from TULM, REVN, and AZU stations. I observe a high seismic activity at these stations from May 17 to May 19, 2015. I applied several filters: [1-5] Hz, [3-5] Hz, [4-16] Hz, [5-10] Hz, [7-15] Hz, [10-35] Hz, and [20-40] Hz, to get the seismic signals. AZU and REVN have almost the same seismic signal due to a slight difference in distance between them. Fig. 16 shows the daily seismicity count recorded by the three seismic stations on May 17, 2015.

For May 18, 2015, the three seismic stations record one significant increase in the amplitude around 7:45 am. (Fig. 17); around 3:00 pm, I can observe the start of a tremor event with a duration of almost six hours. Finally, for May 19, 2015, REVN and AZU stations recorded several amplitude increases during this day, primarily from 1:00 pm to

Figure 16. Filtered seismic signal from El Reventador volcano. I applied a filter between [1 – 5] Hz to the signal. TULM, AZU, and REVN stations recorded this seismic signal on May 17, 2015, from 0:00, am to 11:59 pm.

Figure 17. Filtered seismic signal from El Reventador volcano. I applied a filter between [1–5] Hz to the signal. TULM, AZU, and REVN stations recorded this seismic signal on May 18, 2015, from 0:00, am to 11:59 pm.
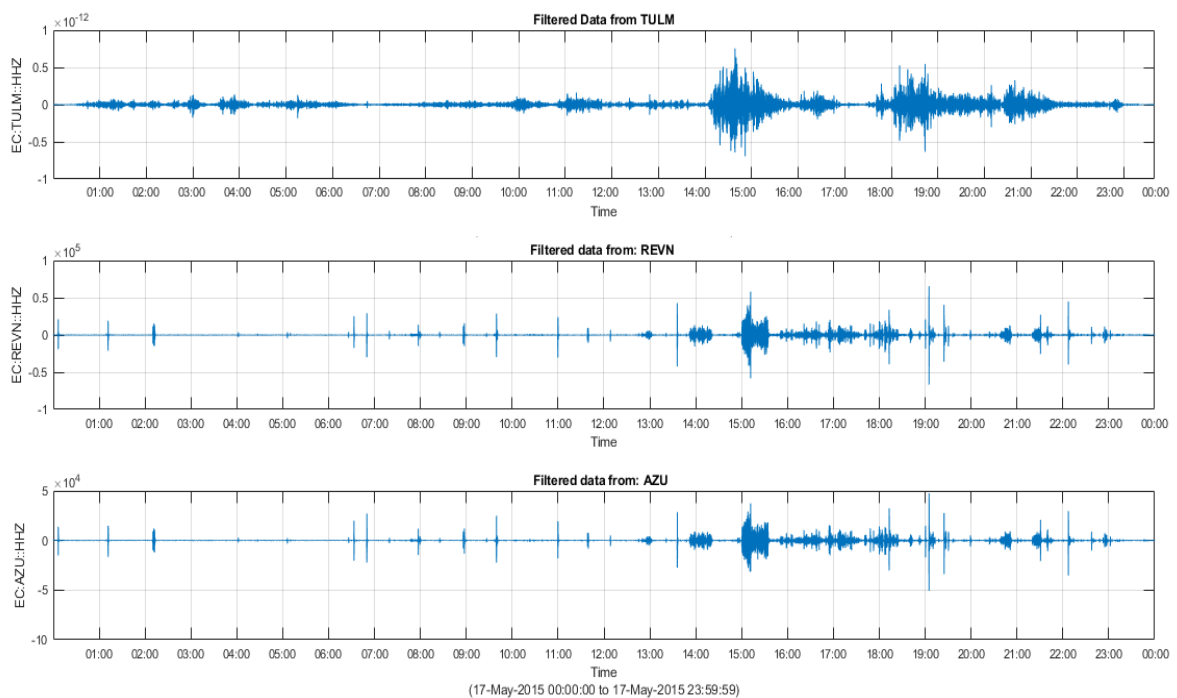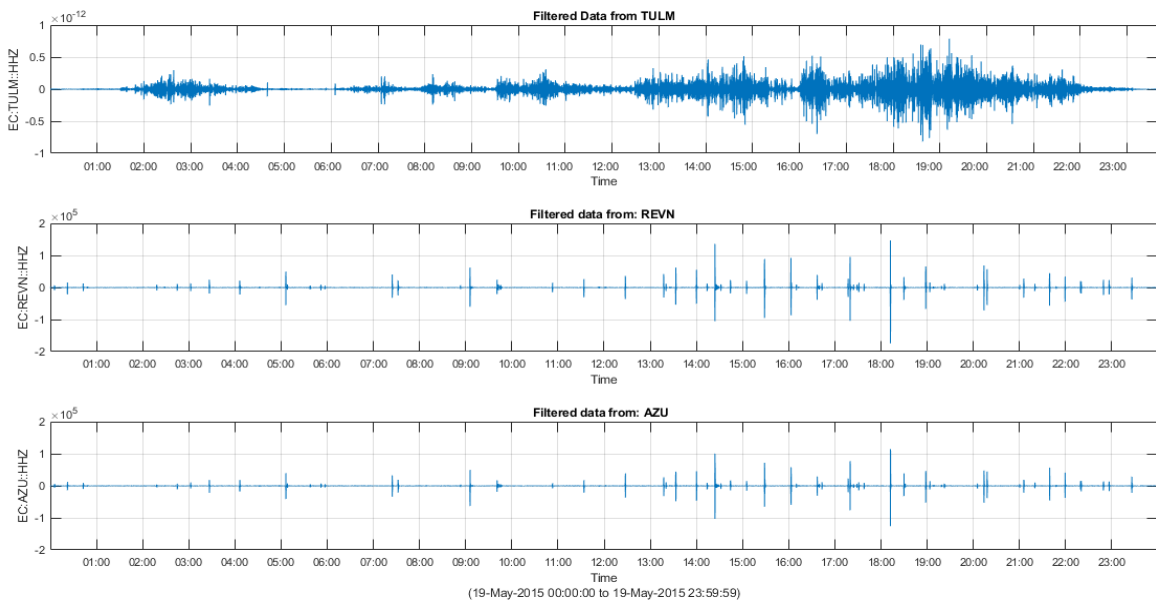

Figure 18. Filtered seismic signal from El Reventador volcano. I applied a filter between [1 – 5] Hz to the signal. TULM, AZU, and REVN stations recorded this seismic signal on May 19, 2015, from 0:00, am to 11:59 pm
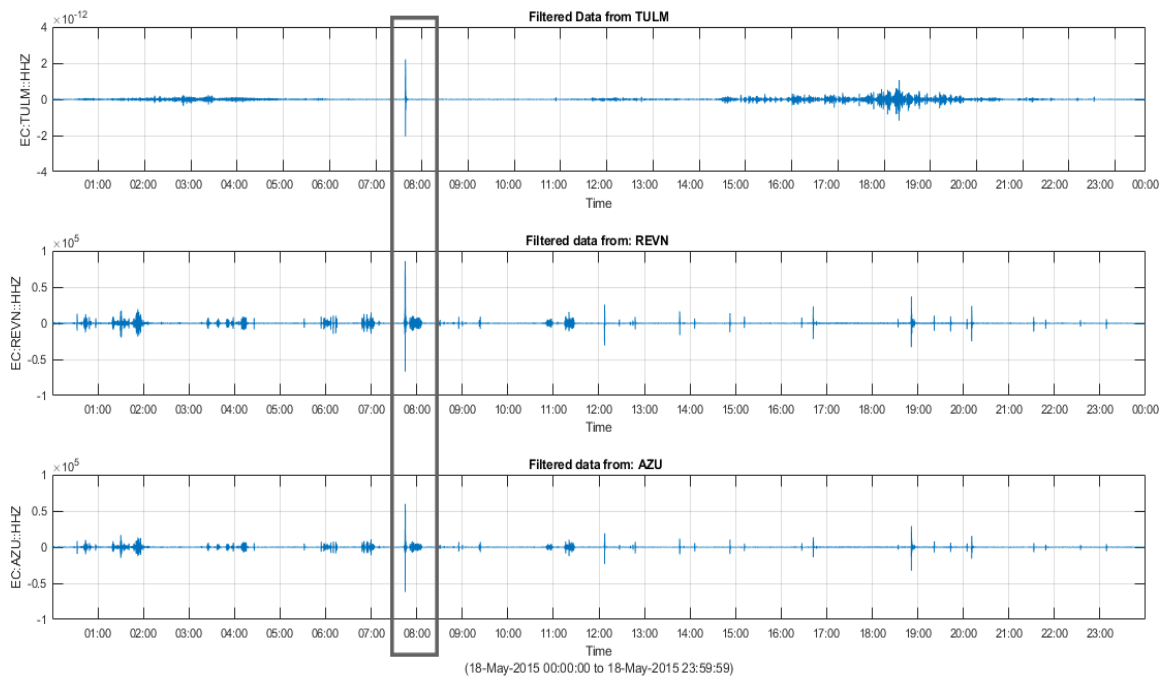
8. Discussion

8.1 Infrasound events from El Reventador volcano

With an initial focus on the time period from May to June 2015, I can see two clear short-term events detected in the infrasound signals, which are related to emission tremors associated with lava flows (Fig. 3). Two days before the emission tremors related to lava flows, there was an increase in activity in the number of explosions and tremors. After this, there was a continuous tremor and the descent of lava flow along the volcano's southern flanks. On both days, May 19 and June 24, the amount of lava extrusion reached lengths greater than 1000m.

The classical eruptions at El Reventador volcano are strombolian or vulcanian eruptions with the typical generation of pyroclastic density currents and lava flows (Vallejo, 2017). On Julian day 137 (May 17, 2015), I counted 150 events between tremors and explosions. On this day, there is a continuous and prolonged signal followed by two successive explosions, with a back azimuth of 258° (Fig. 19). The long and prolonged infrasound signal could be related to an emission tremor which in turn is related to an emplacement of a lava flow. The successive explosions (short duration signals) could be associated with a strombolian activity like in the Tungurahua volcano, where the strombolian activity is related to the emplacement of the lava flow at the surface (Ortiz et al., 2018; Ortiz et al., 2021) and with short-duration, frequent explosions producing jets of gas and magma fragments (Fee and Matoza, 2013).
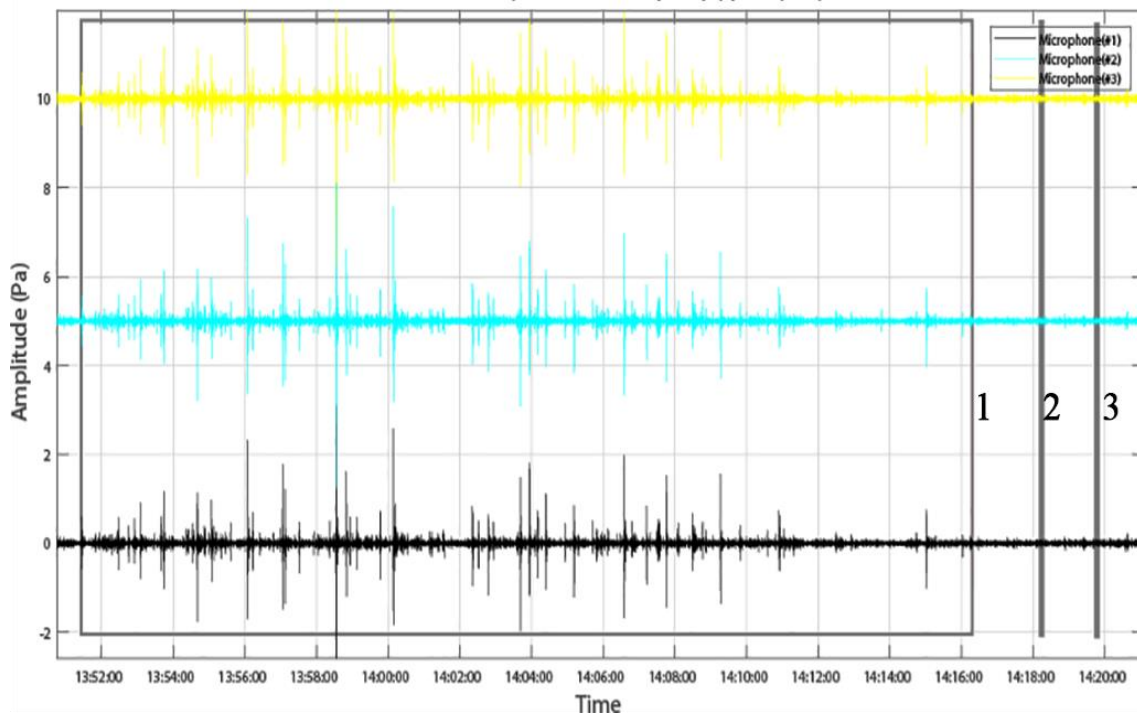
Figure 19. Approximately 30 minutes of infrasound signal from station AZU on day Julian day 137. I identify three separate events: (1): Gray rectangle shows the continuos and prolonged signal; (2),(3): Gray bands shows too short signals. The continuous and prolonged signal with 258° back azimuth has a duration of 25 minutes. Later, two short impulsive signals occur, with a duration of less than one minute and with back azimuths of 258°, and 267° respectively.

8.2 Comparison of the frequency content of El Reventador Events

I estimate the power spectrum and the averaged spectrum for the three seismic stations, from May 17 to May 19, 2015. Fig. 20A-C shows the power spectrum taken from the seismic signal of an all-day activity of May 17, and Fig. 20D shows the averaged spectrum of the same day. Here, I can differentiate the increase of energy related to emission tremors and explosions. Indeed, the most growth of power is related to the emission tremor.
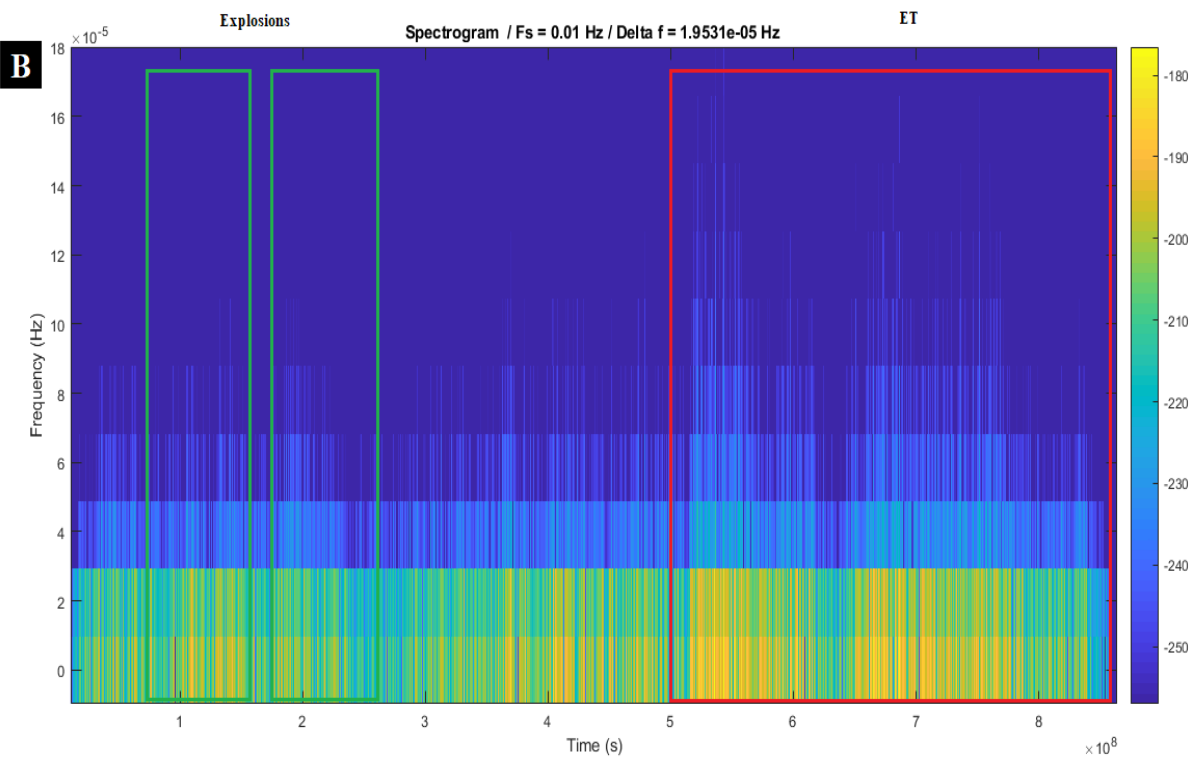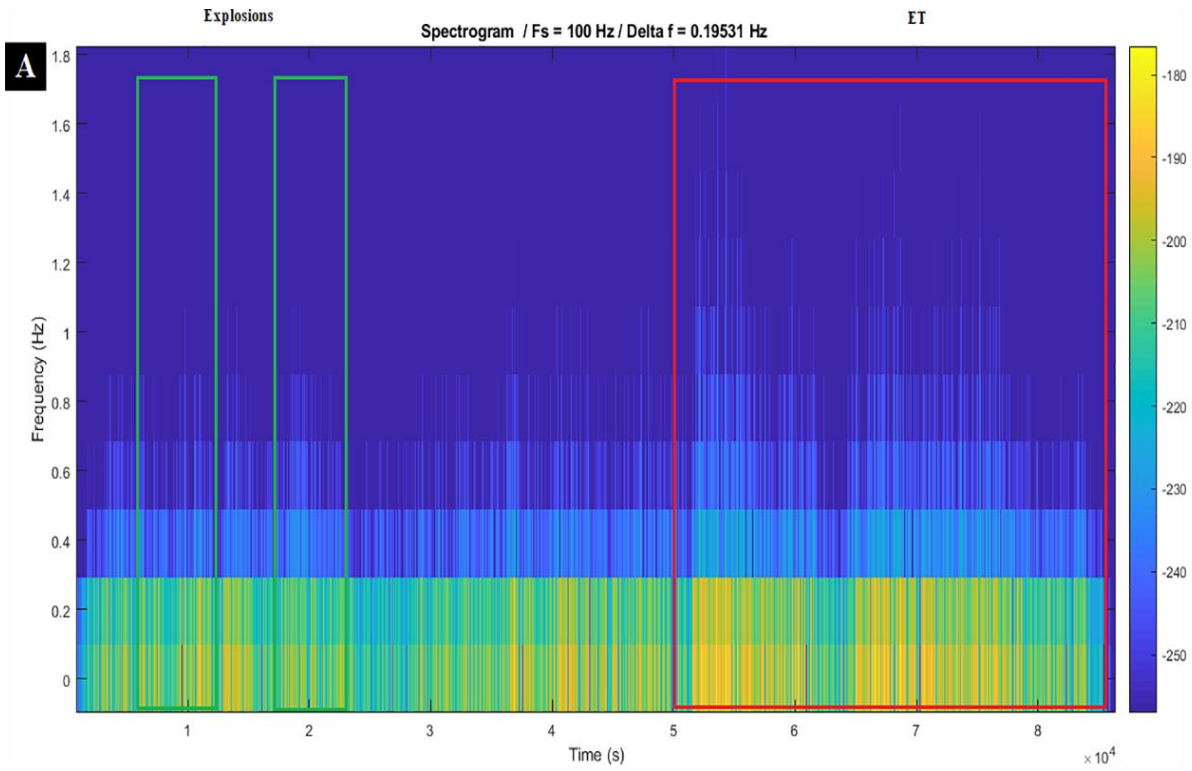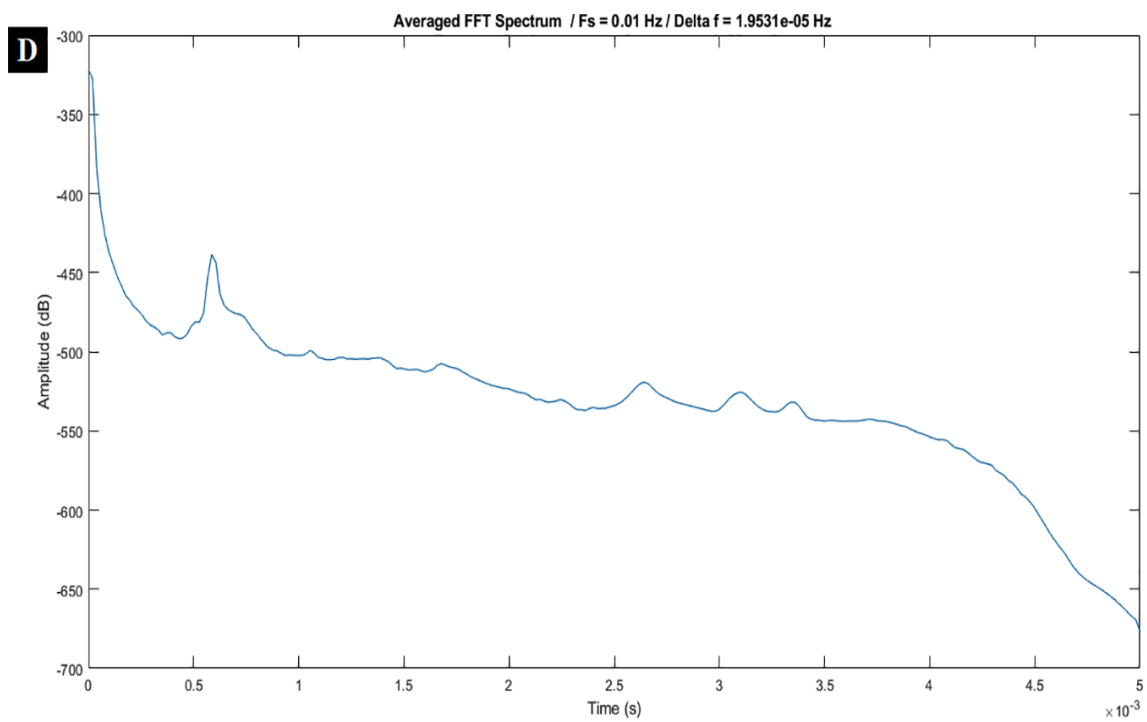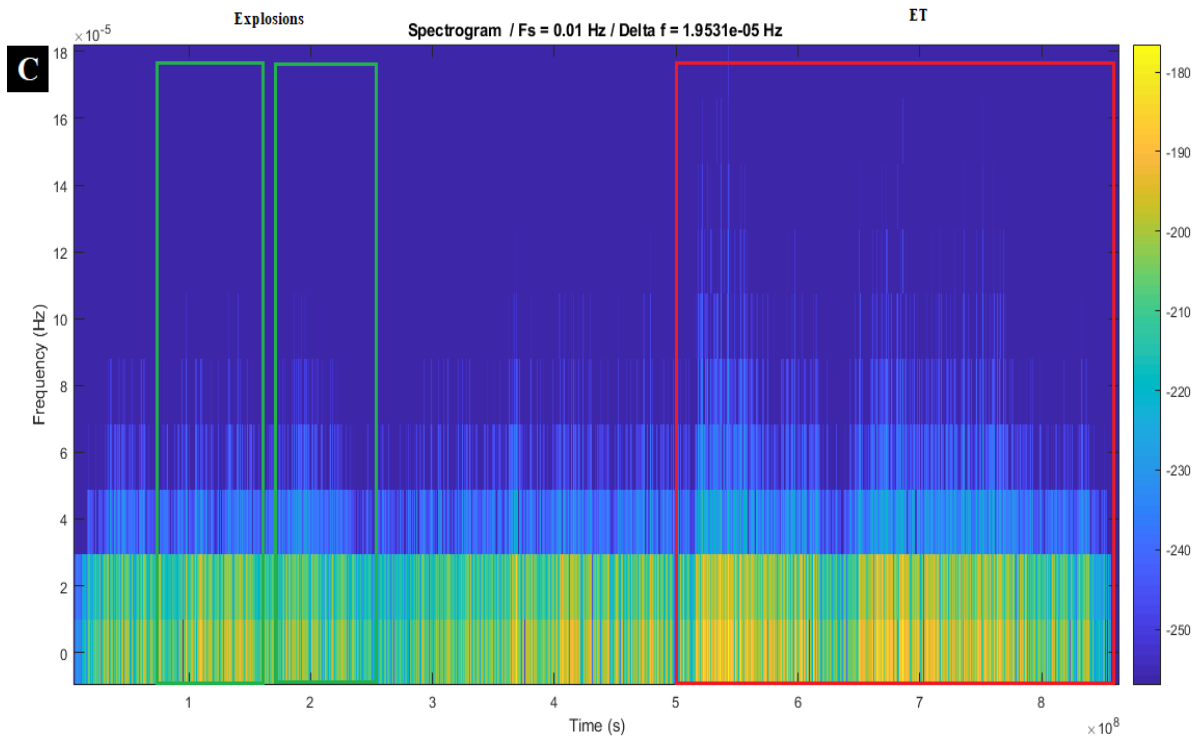
Figure 20. Spectrum and averaged spectrum of seismic signal from El Reventador volcano on May 17. **(A)** Power spectrum through time of the seismic signal from TULM station. I can see a significant increase of energy from 0 to 0.3 Hz. **(B)** Power spectrum through time of the seismic signal from AZU station. I can see a significant increase of energy from 0 to $3x10^{-5}$ Hz. **(C)** Power spectrum through time of the seismic signal from REVN station. I can see a

significant increase of energy from 0 to 3×10^{-5} Hz **(D)** Averaged power spectrum of the seismic signal from AZU station on May 17, 2015. In (A), (B), and (C), the green rectangles show explosions, and red rectangles are emission tremors.

I can see an increase of amplitude in the seismic signal at station CONE of IG-EPN on May 17, 2015. From 1:50 pm, I see a sustained rise in amplitude related to an emission tremor. Besides, I can see short impulses at 1:40 am, 2:28 am, and 4:35 am related to explosions (Fig. 21).
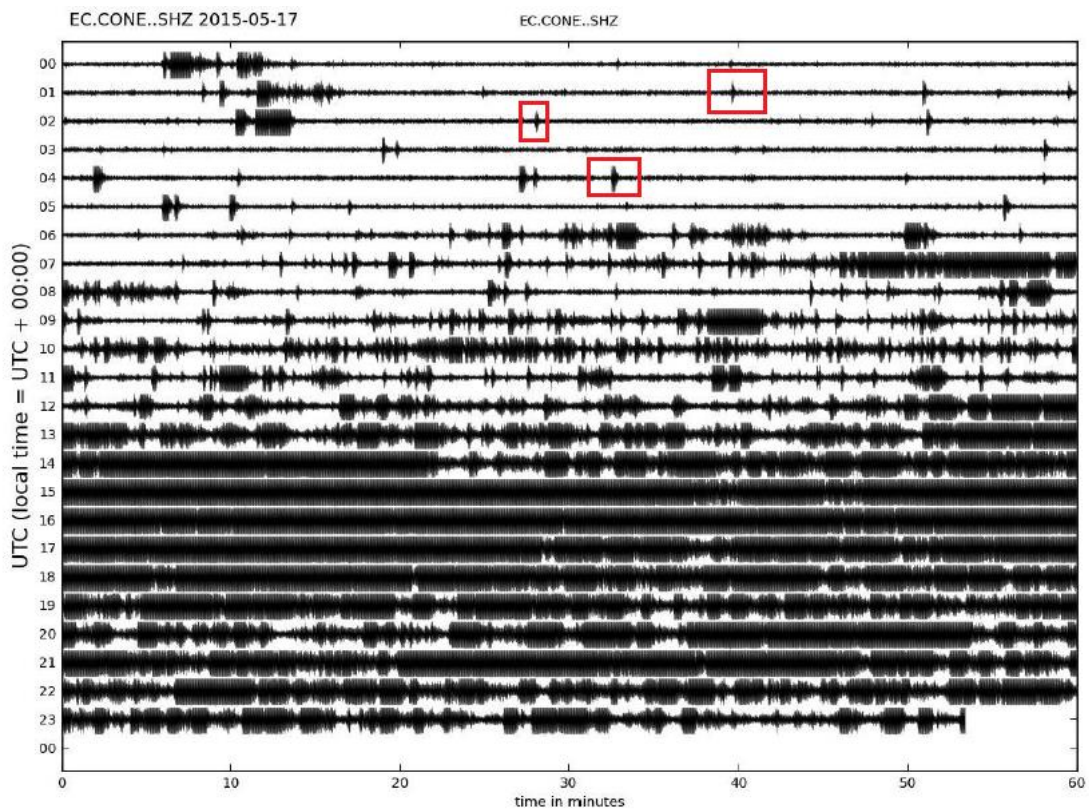
Figure 21. Seismogram of CONE station located on the NE flank of the cone of El Reventador volcano on May 17, 2015. Seismogram taken from Reventador Volcano Special Report N ° 2 IG-EPN, May 19, 2015. From 1:50 pm, there is a sustained rise in amplitude related to a continuous emission tremor. The three red boxes show short impulses at 1:40 am, 2:28 am, and 4:35 am related to explosions.

8.3 Comparison of infrasound and seismic signals

I can classify explosions as simple impulses of short-duration of less than 1 minute (Fig. 12B and Fig. 13B), and tremors as impulses of long-duration of approximately 5 minutes (Johnson & Less, 2000) (Fig. 19 and Fig. 15B). El Reventador volcano's seismic activity is commonly tremors, explosions, and long-period events (Table 1). I find visible tremor events on the seismic signals (Fig. 16, Fig. 18, and Fig. 22A) which have a duration from minutes to hours. These tremors are related to the movement of fluids inside the volcanic conduit (Vallejo, 2017).
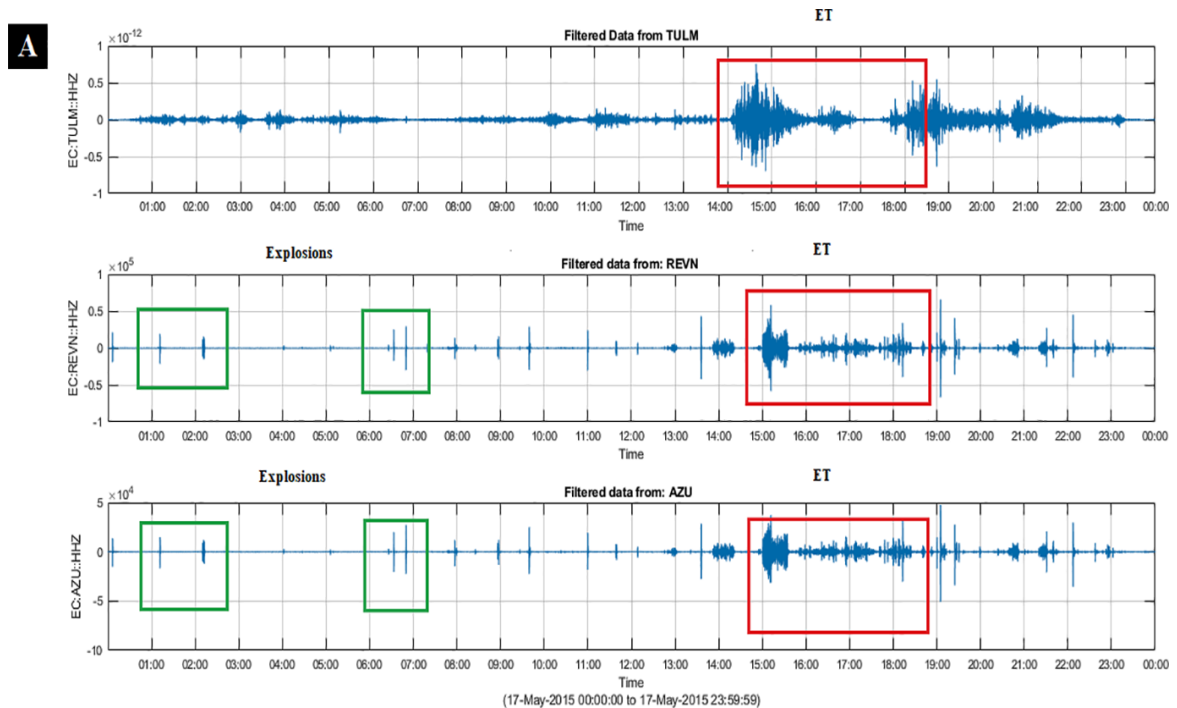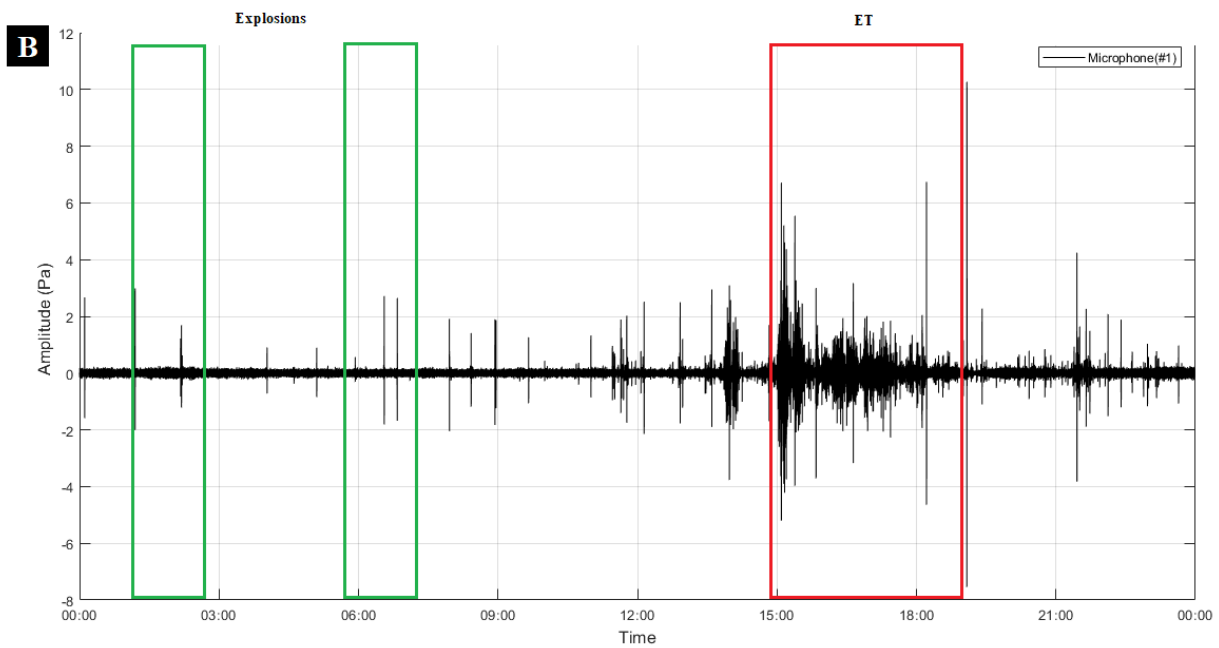
Figure 22. Seismic and infrasound signal on Julian day 137 (May 17, 2015). **(A)** Seismic signal from TULM, REVN, and AZU stations. From 2:54 pm, AZU and REVN stations recorded an emission tremor (ET) event marked by the red boxes. TULM station recorded a tremor from 2:10 pm. Explosions are marked with green boxes. **(B)** Infrasound signal from microphone 1 of AZU infrasound array. From 2:54 pm, microphone 1 records the same emission tremor event, marked by the red box. Explosions are marked with green boxes.

The three seismic stations (TULM, AZU, and REVN) and AZU infrasound array recorded the tremor events. Fig. 22 shows the infrasound and seismic signals' similarity on the tremor event registered on May 17, 2015. Although TULM station is far away from El Reventador volcano (~90 km), it can accurately record the tremor-related to possible movement and effusion of lava. AZU and REVN stations also recorded the tremor event seen on the infrasound signal (Fig. 19). Then, based on the duration of the signal, I can ratify that this signal is associated with an emission tremor which in turn is related to an emplacement of the lava flow.

On the contrary, the signals with shorter duration can be related to gas emissions and explosions. The period of explosions goes from seconds to minutes, much shorter in duration than tremors. The two closer seismic stations and AZU infrasound array can record the explosions from El Reventador volcano; in fig. 22, I can see very short impulses related to explosions and gas emissions.

8.4 Hazards monitoring and risk mitigation

Since 2002, the volcanic activity of El Reventador represents a major source of hazard to the population, infrastructure, and environment of the Sub-Andean region of Ecuador. Currently, El Reventador is monitored by the Instituto Geofísico de la Escuela Politécnica Nacional (IG-EPN). Here, I show a complement and an important tool to study the dynamics and behaviour of the active volcanoes. This tool, the infrasound, can record emission tremors and explosions, which helps assess the hazard and risk on El Reventador. I showed an infrasound catalog where I differentiated type of events, as emission tremors and explosions. Besides, I can determine the source of infrasound extracting their back azimuth: El Reventador (250° to 270°) and San Rafael waterfall (~110°).

Local infrasound is an essential monitoring tool that can characterize, detect, and quantify volcanic eruptive activity. For instance, infrasound is the only tool able to measure the disturbance of the atmosphere. Infrasound can contribute to the study of volcanic activity when other instruments of monitoring are not available. For example, El Reventador is continuously covered by clouds which makes it nonviable for the visual monitoring. Moreover, seismic stations capture only the disturbance in the solid earth, but they cannot record the acceleration of gasses on the atmosphere. Hence, the merge of infrasound to the network monitoring strengthens the assessment of hazard and risk produced by the volcanic activity of El Reventador.

9. Conclusions

The main objective of this work was to build an infrasound catalog and compare infrasound with seismic signals. To accomplish this goal, I 1) collected and processed data taken from AZU infrasound array located at 'local distances' (less than << 15 km from the summit of El Reventador), 2) tested and applied different frequency ranges and parameters of time such as window length and gap, and 3) compared the infrasound signals with the seismic data and volcanic activity reported by IGEPN.

El Reventador volcano is currently one of the most active volcanoes in the Ecuadorian arc since it reactivated its volcanic activity in 2002. Its exploding activity represents a significant source of hazard, and its geomorphology has been evolving rapidly due to continuous activity through the last 17 years. The dynamics of eruptions of this volcano are chiefly the phases of volcanic quiescence and eruptions over long periods, which produces quasi-continuous and intense acoustic activity. I demonstrate that infrasound waves generated at El Reventador volcano can be used to monitor the volcanic activity. I also relate the infrasound signals with the seismic activity, which can help identify the type of activity occurring.

I have performed parameter testing to identify the frequency ranges and consistency criteria that best detect events for this area and examined the detected events as a function of back azimuth to separate the two central sources of infrasound: the volcano and San Rafael waterfall. Most events associated with El Reventador volcano were identified in the frequency range of [10-35] Hz. I show a new catalog of infrasound events from El Reventador volcano [1-5] Hz from May 1, 2015, to June 30, 2015.

Bibliography

Almeida, M., H. E. Gaunt, and P. Ramón (2019), Ecuador's El Reventador volcano continually remakes itself, Eos, 100, https://doi.org/10.1029/2019EO117105. Published on 18 March 2019.

Alvarado, A., Ruiz, M., Mothes, P., Yepes, H., Segovia, M., Vaca, M., ... & Córdova, A. (2018). Seismic, volcanic, and geodetic networks in Ecuador: Building capacity for monitoring and research. Seismological Research Letters, 89(2A), 432-439.

Arnold, D. W. D., Biggs, J., Anderson, K., Vallejo Vargas, S., Wadge, G., Ebmeier, S. K., ... & Mothes, P. (2017). Decaying Lava Extrusion Rate at El Reventador Volcano , Ecuador , Measured Using High-Resolution. 9966–9988

Arnold, D. W., Biggs, J., Dietterich, H. R., Vargas, S. V., Wadge, G., & Mothes, P. (2019). Lava flow morphology at an erupting andesitic stratovolcano: A satellite perspective on El Reventador, Ecuador. Journal of Volcanology and Geothermal Research, 372, 34-47.

Benoit, J. P., & McNutt, S. R. (1997). New constraints on source processes of volcanic tremor at Arenal Volcano, Costa Rica, using broadband seismic data. Geophysical Research Letters, 24(4), 449-452.

Braun, T., & Ripepe, M. (1993). Interaction of seismic and air waves recorded at Stromboli Volcano. Geophysical Research Letters, 20(1), 65–68. https://doi.org/10.1029/92GL02543

Cansi, Y. (1995). An automatic seismic event processing for detection and location: The PMCC method. Geophysical research letters, 22(9), 1021-1024.

Evers, L. G., & Haak, H. W. (2003). Tracing a meteoric trajectory with infrasound. Geophysical Research Letters, 30(24).

Fee, D., & Matoza, R. S. (2013). An overview of volcano infrasound: From hawaiian to plinian, local to global. Journal of Volcanology and Geothermal Research, 249, 123–139. https://doi.org/10.1016/j.jvolgeores.2012.09.002

Garcés, M., Bass, H., Drop, D., Hetzer, C., Hedlin, M., Le Pichon, A., ... & Olson, J. (2004). Forensic studies of infrasound from massive hypersonic sources. Eos, Transactions American Geophysical Union, 85(43), 433-441.

Garcés, M., Caron, P., Hetzer, C., Le Pichon, A., Bass, H., Drob, D., & Bhattacharyya, J. (2005). Deep infrasound radiated by the sumatra earthquake and tsunami. Eos, 86(35). https://doi.org/10.1029/2005EO350002

Hagerty, M. T., Schwartz, S. Y., Garcés, M. A., & Protti, M. (2000). Analysis of seismic and acoustic observations at Arenal Volcano, Costa Rica, 1995-1997. Journal of Volcanology and Geothermal Research, 101(1–2), 27–65. https://doi.org/10.1016/S0377-0273(00)00162-1

Hall M, Ramon P, Mothes P, LePennec JL, Garcia A, Samaniego P, Yepes H. Volcanic eruptions with little warning: the case of Volcán Reventador's Surprise November 3, 2002 Eruption, Ecuador. Revista geológica de Chile. 2004;31(2):349–58

Instituto Geofísico de la Escuela Politécnica Nacional (IGEPN), 2020 . Volcán Reventador: Informes Diarios. Quito. Retrieved from: https://www.igepn.edu.ec/reventador-informes/rev-diarios.

Instituto Geofísico de la Escuela Politécnica Nacional (IGEPN), 2021. Volcán El Reventador. Quito.

Johnson, J. B., & Lees, J. M. (2000). Plugs and chugs - seismic and acoustic observations of degassing explosions at Karymsky, Russia and Sangay, Ecuador. Journal of Volcanology and Geothermal Research, 101(1–2), 67–82. https://doi.org/10.1016/S0377-0273(00)00164-5

Johnson, J. B., Aster, R. C., Ruiz, M. C., Malone, S. D., McChesney, P. J., Lees, J. M., & Kyle, P. R. (2003). Interpretation and utility of infrasonic records from erupting volcanoes. Journal of volcanology and geothermal research, 121(1-2), 15-63.

Johnson, Jeffrey B., Lees, J. M., & Yepes, H. (2006). Volcanic eruptions, lightning, and a waterfall: Differentiating the menagerie of infrasound in the Ecuadorian jungle. Geophysical Research Letters, 33(6), 23–26. https://doi.org/10.1029/2005GL025515

Johnson, J. B., & Ripepe, M. (2011). Volcano infrasound: A review. Journal of Volcanology and Geothermal Research, 206(3–4), 61–69. https://doi.org/10.1016/j.jvolgeores.2011.06.006

Lees, J. M., Johnson, J. B., Ruiz, M., Troncoso, L., & Welsh, M. (2008). Reventador Volcano 2005: Eruptive activity inferred from seismo-acoustic observation. Journal of Volcanology and Geothermal Research, 176(1), 179–190. https://doi.org/10.1016/j.jvolgeores.2007.10.006

Matoza, R. S., Hedlin, M. A. H., & Garcés, M. A. (2007). An infrasound array study of Mount St. Helens. Journal of Volcanology and Geothermal Research, 160(3–4), 249–262. https://doi.org/10.1016/j.jvolgeores.2006.10.006

Muñoz Di-parodi, J. C. (2002). Introducción a los Infrasonidos y su Recepción. 105

Naranjo, M. F., Ebmeier, S. K., Vallejo, S., Ramón, P., Mothes, P., Biggs, J., & Herrera, F. (2016). Mapping and measuring lava volumes from 2002 to 2009 at El Reventador Volcano, Ecuador, from field measurements and satellite remote sensing. Journal of Applied Volcanology, 5(1). https://doi.org/10.1186/s13617-016-0048-z

Ortiz, H. D., & Johnson, J. B. (2013). Multi-year infrasound deployment at Volcán El Reventador [Data set]. International Federation of Digital Seismograph Networks. https://doi.org/10.7914/SN/6M_2013

Ortiz, H. D., Johnson, J. B., Ramón, P. G., & Ruiz, M. C. (2018). Using infrasound waves to monitor tropospheric weather and crater morphology changes at Volcán Tungurahua, Ecuador. Journal of Volcanology and Geothermal Research, 349, 205–216. https://doi.org/10.1016/j.jvolgeores.2017.11.001

Ortiz H. D., Matoza R. S., Garapaty C., Rose K., Ramón P., and Ruiz M., (2020). Multi-year regional infrasound detection of Tungurahua, El Reventador, and Sangay volcanoes in Ecuador from 2006 to 2013. Proceedings of Meetings in Acoustics, 41, 022003.

Ortiz, H. D., Matoza, R. S., Johnson, J. B., Hernandez, S., Anzieta, J. C., & Ruiz, M. C. (2021). Autocorrelation infrasound interferometry. Journal of Geophysical Research: Solid Earth, 126, e2020JB020513. https://doi.org/10.1029/2020JB020513

Oshima, H., Maekawa, T., 2001. Excitation process of infrasonic waves associated with Merapi-type pyroclastic flow as revealed by a new recording system. Geophysical Research Letters 28 (6), 1099–1102.

Pierce, A.D., 1981. Acoustics—An introduction to Its Physical Principles and Applications. McGraw-Hill, New York.

Ripepe, M., Marchetti, E., Bonadonna, C., Harris, A.J.L., Pioli, L., Ulivieri, G., 2010. Mono-chromatic infrasonic tremor driven by persistent degassing and convection at Villarrica Volcano, Chile. Geophysical Research Letters 37, L15303. http://dx.doi.org/10.1029/2010gl043516.

Rogers, J. A., & Stephens, C. D. (1995). SSAM: real-time seismic spectral amplitude measurement on a PC and its application to volcano monitoring. Bulletin - Seismological Society of America, 85(2), 632–639.

Rost, S., & Thomas, C. (2009). Improving seismic resolution through array processing techniques. Surveys in Geophysics, 30(4–5), 271–299. https://doi.org/10.1007/s10712-009-9070-6

Samaniego, P., Eissen, J. P., Le Pennec, J. L., Robin, C., Hall, M. L., Mothes, P., … Cotten, J. (2008). Pre-eruptive physical conditions of El Reventador volcano (Ecuador) inferred from the petrology of the 2002 and 2004-05 eruptions. Journal of Volcanology and Geothermal Research, 176(1), 82–93. https://doi.org/10.1016/j.jvolgeores.2008.03.004

Vallejo Vargas, S. (2017). Numerical models of volcanic flows for an estimation and delimitation of volcanic hazards, the case of Reventador volcano (Ecuador). 227.

Vallejo Vargas, S., Hernandez, S., Hidalgo, S., Vasconez, F., Battaglia, J., Córdova, J., & Proano, A. (2019). Thermal imaging, seismo-acoustic signals and SO2 degasification following a partial summit collapse at El Reventador volcano, Ecuador. In *8ème Symposiumsur la géodynamique des Andes (ISAG)*.

Vélez, M., & Alberto, L. (2011). Análisis de señales sísmicas y de infrasonido tipo chugging asociadas a la emisión de gases en el volcán el reventador (Bachelor's thesis, QUITO/EPN/2011).

Annexes

Table 4. Local Infrasound catalog of the events of El Reventador volcano using the frequency range [1-5] Hz, a window length of 3 s and a gap value of 60 s.

Date	Julian Day	Number of events	Date	Julian Day	Number of events
1/5/2015	121	111	1/6/2015	152	70
2/5/2015	122	126	2/6/2015	153	92
3/5/2015	123	125	3/6/2015	154	76
4/5/2015	124	73	4/6/2015	155	72
5/5/2015	125	108	5/6/2015	156	93
6/5/2015	126	62	6/6/2015	157	62
7/5/2015	127	98	7/6/2015	158	38
8/5/2015	128	147	8/6/2015	159	63
9/5/2015	129	125	9/6/2015	160	86
10/5/2015	130	92	10/6/2015	161	62
11/5/2015	131	47	11/6/2015	162	76
12/5/2015	132	65	12/6/2015	163	54
13/5/2015	133	46	13/6/2015	164	54
14/5/2015	134	59	14/6/2015	165	58
15/5/2015	135	80	15/6/2015	166	51
16/5/2015	136	104	16/6/2015	167	49
17/5/2015	137	150	17/6/2015	168	45
18/5/2015	138	112	18/6/2015	169	20
19/5/2015	139	76	19/6/2015	170	55
20/5/2015	140	103	20/6/2015	171	52
21/5/2015	141	111	21/6/2015	172	59
22/5/2015	142	66	22/6/2015	173	48
23/5/2015	143	50	23/6/2015	174	115
24/5/2015	144	45	24/6/2015	175	95
25/5/2015	145	41	25/6/2015	176	32
26/5/2015	146	58	26/6/2015	177	34
27/5/2015	147	74	27/6/2015	178	58
28/5/2015	148	76	28/6/2015	179	40
29/5/2015	149	85	29/6/2015	180	40
30/5/2015	150	71	30/6/2015	181	40
31/5/2015	151	91			

To see the full data of infrasound catalog, please contact to: jorge.perea.armijos@gmail.com

Annex. Table A1. Activity of El Reventador volcano of May 2015. Data taken from daily reports of Instituto Geofísico de la Escuela Politécnica Nacional.

DATE	VT	LP	Explosions	Tremors	Rains	Lahars	Vapor Mts-direction	Observations	TE	TA
1/5/2015	1	38	60	6	YES	NO	500 -C	ASH & STEAM	6	
2/5/2015		32	45	2	NO	NO		CLOUDY	2	
3/5/2015		23	32	6	NO	NO	200 -C	WATER STEAM	6	
4/5/2015		20	25	7	YES	NO		CLOUDY	5	2
5/5/2015		39	36	8	YES	NO	1000 -W	ASH & GLOW	8	3
6/5/2015		22	27	4	YES	NO		CLOUDY	4	5
7/5/2015		51	54	2	YES	NO		CLOUDY & GLOW	2	0
8/5/2015		106	61	6	YES	NO	1000 -C	GLOW	6	0
9/5/2015		36	31	20	YES	NO	500 -C	WATER STEAM	16	4
10/5/2015		20	30	46	YES	NO		CLOUDY	12	27
11/5/2015		45	29	35	YES	NO		CLOUDY	15	20
12/5/2015		49	30	37	YES	NO		CLOUDY	18	19
13/5/2015		33	18	15	YES	NO		CLOUDY	11	4
14/5/2015		25	20	13	YES	NO		CLOUDY	5	8
15/5/2015		23	26	6	YES	NO		CLOUDY	2	4
16/5/2015		31	38	6	YES	NO		GLOW	4	2
17/5/2015		99	38	5	YES	NO		CLOUDY	2	3
18/5/2015		42	21	11	YES	NO		LAVA FLOW UNDER THE CRATER	9	2
19/5/2015		38	35	4	NO	NO	200 -NW	LAVA FLOW IN SOUTHERN FLANK VOLCANO - THERMAL IMAGE CHECK	4	0
20/5/2015		107	45	15	YES	NO		LAVA FLOW IN SOUTHERN FLANK VOLCANO - THERMAL IMAGE CHECK	15	0
21/5/2015		37	38	7	YES	NO		DESCENT OF LAVA FLOW BY THE SOUTH FLANK	4	3
22/5/2015		35	47	25	NO	NO		CLOUDY	9	16
23/5/2015		42	28	23	NO	NO		CLOUDY	6	17
24/5/2015		47	30	7	YES	NO	600 -SW	ASH	5	2
25/5/2015		37	29	9	YES	NO	800 -SW	ASH	6	3
26/5/2015		16	29	8	YES	NO	1500 -SW	WATER STEAM	8	0
27/5/2015		33	19	4	NO	NO	1000 -SE	CLOUDY	2	2
28/5/2015		74	27	3	NO	NO	800 -NW	ASH	3	0
29/5/2015		39	20	4	NO	NO	600 -NW	ASH	2	2
30/5/2015		55	25	12	NO	NO	1000 -SW	ASH	2	7
31/5/2015		40	34	30	YES	NO		CLOUDY	8	22

Annex. Table A2. Activity of El Reventador volcano of June 2015. Data taken from daily reports of Instituto Geofísico de la Escuela Politécnica Nacional.

DATE	VT	LP	Explosions	Tremors	Rains	Lahars	Vapor Mts-direction	Observations	TE	TA
1/6/2015		86	26	10	YES	NO	1000 -NW	CLOUDY	10	0
2/6/2015		46	30	9	NO	NO	300 -NW		5	4
3/6/2015		26	26	12	NO	NO		CLOUDY	5	7
4/6/2015		48	21	11	YES	NO		CLOUDY	2	9
5/6/2015		30	23	14	YES	NO	500 -SW	ASH & STEAM	5	9
6/6/2015		16	19	17	NO	NO		CLOUDY	15	2
7/6/2015		25	23	21	NO	NO		CONTINUOUS DESCENT OF LAVA THROUGH THE WESTERN FLANK AT 1200m BELOW EL CRATER	17	4
8/6/2015		30	19	15	YES	NO	500 -SW	WATER STEAM	14	1
9/6/2015		24	22	6	NO	NO		CLOUDY	5	1
10/6/2015		25	28	11	YES	NO	1000 -C	ASH	8	3
11/6/2015		28	30	27	YES	NO		CLOUDY	9	18
12/6/2015	1	5	10	28	YES	NO	500 -NE	WHITE WATER VAPOR	16	12
13/6/2015		32	28	14	YES	NO	1000 SW	LAVA FLOW IN SOUTHERN FLANK VOLCANO - THERMAL IMAGE CHECK	6	8
14/6/2015	1	22	30	7	NO	NO	1000 -NW	ASH	4	3
15/6/2015		71	26	12	NO	NO		CLOUDY	12	0
16/6/2015		34	22	7	YES	NO		ASH	7	0
17/6/2015		30	19	17	NO	NO		CLOUDY	12	5
18/6/2015		20	15	15	YES	NO		CLOUDY	13	2
19/6/2015		26	21	12	NO	NO		CLOUDY	11	1
20/6/2015		35	25	24	YES	NO		CLOUDY	18	6
21/6/2015		28	27	16	YES	NO		CLOUDY	13	3
22/6/2015		25	28	16	NO	NO		CLOUDY	3	13
23/6/2015		57	9	5	NO	NO		CONTINUOS TREMOR	5	0
24/6/2015				1	YES	NO		CONTINUOUS TREMOR AND FLOW DESCENT	1	
25/6/2015		12	18	2	YES	NO		2 LONG-LASTING TREMOR		
26/6/2015		22	29	17	YES	NO		17 LONG-LASTING TREMOR		
27/6/2015		18	19	10	YES	NO		10 LONG-LASTING TREMOR AND LAVA FLOWS		
28/6/2015		19	35	10	YES	NO		LAVA FLOW DESCENDING THROUGH THE SOUTH FLANK OF THE VOLCANO	10	
29/6/2015		40	17	35	YES	NO	300 -SW	DESCENT OF LAVA FLOW BY THE SOUTH FLANK	10	25
30/6/2015		40	20	4	YES	NO			3	1

Annex. Table A3. Activity of El Reventador volcano of July 2015. Data taken from daily reports of Instituto Geofísico de la Escuela Politécnica Nacional.

DATE	VT	LP	Explosions	Tremors	Rains	Lahars	Vapor Mts-direction	Observations	TE	TA
1/7/2015		45	23	6	YES	NO		INCANDESCENT MATERIAL DESCENDING UP TO 500M	2	2
2/7/2015		53	31	9	YES	NO		INCANDESCENT MATERIAL DESCENDING UP TO 500M	5	4
3/7/2015		68	26	3	YES	NO	2000 -SW	ASH	3	0
4/7/2015		88	33	12	YES	NO		CLOUDY	12	
5/7/2015		61	37	6	YES	NO		CLOUDY	6	0
6/7/2015		37	14	37	YES	NO	500 -SW	DESCENT OF LAVA FLOW BY THE SOUTH FLANK	9	0
7/7/2015		25	10	20	NO	NO		CLOUDY	5	15
8/7/2015		30	23	5	NO	NO		CLOUDY	3	2
9/7/2015		65	15	19	YES	NO		CLOUDY	19	0
10/7/2015		45	12	18	YES	NO		CLOUDY	18	0
11/7/2015		65	42	25	YES	NO		CLOUDY	25	0
12/7/2015		56	28	21	YES	NO		CLOUDY	21	
13/7/2015		31	20	4	YES	NO	1000 -NW	ASH	4	0
14/7/2015		35	25	6	NO	NO	1000 - SW	ASH & STEAM	6	0
15/7/2015		28	22	8	YES	NO		CLOUDY	8	
16/7/2015		49	35	32	NO	NO	1300 NW	ASH	32	
17/7/2015		61	28	23	NO	NO	700 -W	INCANDESCENCE IN THE TOP OF THE CRATER	23	0
18/7/2015		50	35	13	YES	NO			13	
19/7/2015		48	25	25	YES	NO			25	
20/7/2015		30	27	7	YES	NO	1000 -NW	ASH	4	3
21/7/2015	1	33	27	5	NO	NO	1500 -WC	DESCENT OF INCANDESCENT MATERIAL DURING EXPLOSIONS	3	2
22/7/2015	3	54	40	23	YES	NO	500 -NW	ASH	15	8
23/7/2015		45	26	38	YES	NO		ASH & STEAM	10	28
24/7/2015		42	34	22	YES	NO	600 - NW	DESCENT OF LAVA FLOW BY THE SOUTH FLANK	14	8
25/7/2015		47	16	26	YES	NO	1000 -NW	LAVA FLOW IN SOUTHERN FLANK VOLCANO - THERMAL IMAGE CHECK	8	18
26/7/2015		50	36	10	YES	NO		CLOUDY	1	9
27/7/2015		46	39	17	YES	NO		CLOUDY	13	4
28/7/2015		36	22	10	YES	NO		CLOUDY	3	7
29/7/2015		42	20	1	YES	NO		CLOUDY	1	
30/7/2015		39	27	2	YES	NO		CLOUDY	2	
31/7/2015		60	39	44	YES	NO		CLOUDY	27	17